Interleukin 1 upregulates microRNA-135b to promote inflammation-associated gastric carcinogenesis in mice.

Interleukin 1 Upregulates MicroRNA 135b to Promote Inflammation-associated Gastric Carcinogenesis in Mice

Short Title: miR-135b promotes gastritis and tumorigenesis

Tae-Su Han[1,2,3], Dominic Chih-Cheng Voon[1,4*], Hiroko Oshima[1,5], Mizuho Nakayama[1,5], Kanae Echizen[1,2], Eri Sakai[1], Zachary Wei Ern Yong[1], Kazuhiro Murakami[1], Liang Yu[6,7], Toshinari Minamoto[8], Chan-Young Ock[9,10], Brendan J. Jenkins[6,7], Seong-Jin Kim[9,10], Han-Kwang Yang[11] and Masanobu Oshima[1,2,5*]

[1] Division of Genetics, Cancer Research Institute, Kanazawa University, Kanazawa, Japan.

[2] AMED-CREST, AMED, Japan Agency for Medical Research and Development, Tokyo, Japan.

[3] Biotherapeutics Translational Research Center, Division of Biomedical Science, Korea Research Institute of Bioscience and Biotechnology, Daejeon, Korea.

[4] Innovative Cancer Model Research Unit, Institute for Frontier Science Initiative, Kanazawa University, Kanazawa, Japan.

[5] WPI Nano-Life Science Institute (Nano-LSI), Kanazawa University, Kanazawa, Japan.

[6] Centre for Innate Immunity and Infectious Diseases, Hudson Institute of Medical Research, Monash University, Clayton, Australia.

[7] Department of Molecular Translational Science, School of Clinical Sciences, Monash University, Clayton, Australia.

[8] Division of Translational and Clinical Oncology, Cancer Research Institute, Kanazawa University, Kanazawa, Japan.

[9] Theragen Etex Bio Institute, Suwon, Korea.

[10] Precision Medicine Research Center, Advanced Institutes of Convergence Technology and Department of Transdisciplinary Studies, Seoul National University, Suwon, Korea.

[11] Department of Surgery and Cancer Research Institute, Seoul National University College of Medicine, Seoul, Korea.

[*] Corresponding authors

Grant support:

This research is supported by the AMED-CREST (JP17gm0410014) and AMED (JP17ck0106259) from the Japan Agency for Medical Research and development, AMED; and by a Grants-in-Aid for Scientific Research (A) (JP15H02362, JP18H04030; M.O.) and a Grants-in-Aid for Scientific Research (C) (JP18K07228; D.C.V) from the Ministry of Education, Culture, Sports, Science and Technology of Japan; and by National Research Foundation of Korea (NRF) grants funded by the Korean government (NRF-2017R1C1B2012268; T-S.H.) and KRIBB Research Initiative Program.

Abbreviations: miRNA, microRNA; GC, gastric cancer

Corresponding authors:

Dominic Voon, Innovative Cancer Model Research Unit, Institute for Frontier Science Initiative; and Division of Genetics, Cancer Research Institute, Kanazawa University,

Kanazawa, Ishikawa 920-1192, Japan. Phone: 81-76-264-6792; Fax: 81-76-234-4519; E-mail: dvoon@staff.kanazawa-u.ac.jp

Masanobu Oshima, Division of Genetics, Cancer Research Institute, Kanazawa University, Kanazawa, Ishikawa 920-1192, Japan. Phone: 81-76-264-6760; Fax: 81-76-234-4519; E-mail: oshimam@staff.kanazawa-u.ac.jp

Disclosures:

The authors declare no conflict of interest.

Authors Contribution

T-S.H., D.C.V., H.O. and Z.W.E.Y. performed the experiments; H.O., K.E., M.N., E.S. and K.M. provided technical support and assisted in data analysis; L.Y., B.J. C-Y.O. and S-J.K. assisted in bioinformatics and statistical analyses; T.M. provided clinical samples; B.J. and H-K.Y. contributed to the study concept; T-S.H., D.C.V. and M.O. designed the study concept, interpreted data and prepared the manuscript; M.O. and D.C.V. obtained funding for the study.

Key words: *stomach cancer, carcinogenesis, tumor progression, oncogene*

ABSTRACT

Background & Aims: Gastritis is associated with development of stomach cancer, but little is known about changes in microRNA expression patterns during gastric inflammation. Specific changes in gene expression in epithelial cells are difficult to monitor due to the heterogeneity of the tissue. We investigated epithelial cell-specific changes in microRNA expression during gastric inflammation and gastritis-associated carcinogenesis in mice.

Methods: We used laser microdissection to enrich epithelial cells from K19-C2mE transgenic mice, which spontaneously develop gastritis-associated hyperplasia, and Gan mice, which express activated prostaglandin E2 and Wnt in the gastric mucosa and develop gastric tumors. We measured expression of epithelial cell-enriched microRNAs and used bioinformatics analyses to integrate data from different systems to identify inflammation-associated microRNAs. We validated our findings in gastric tissues from mice, and evaluated protein functions in gastric cell lines (SNU-719, SNU-601, SNU-638, AGS, and GIF-14) and knockout mice. Organoids were cultured from gastric corpus tissues of wild type and miR-135b knockout C57BL/6 mice. We measured levels of microRNAs in pairs of gastric tumors and non-tumor mucosa from 28 patients in Japan.

Results: We found microRNA 135b (MIR135B) to be the most over-expressed microRNA in gastric tissues from K19-C2mE and Gan mice—levels increased during early stages of gastritis-associated carcinogenesis. Levels of MIR135B were also increased in gastric tumor tissues from *gp130*$^{F/F}$ mice and patients, compared with non-tumor tissues. In gastric organoids and immortalized cell lines, expression of MIR135B was induced by interleukin 1 (IL1) signaling. K19-C2mE mice with disruption of *Mir135b* developed hyperplastic lesions that were 50% smaller than mice without *Mir135b* disruption, and had significant reductions

in cell proliferation. Expression of MIR135B in gastric cancer cell lines increased their colony formation, migration, and sphere formation. We identified *FOXN3* and *RECK* mRNAs as targets of MIR135B; their knockdown reduced migration of gastric cancer cell lines. Levels of *FOXN3* and *RECK* mRNAs correlated inversely with levels of MIR135B in human gastric tumors and in inflamed mucosa from K19-C2mE mice.

Conclusions: We found expression of MIR135B to be upregulated by IL1 signaling in gastric cancer cells and organoids. MIR135B promotes invasiveness and stem-cell features of gastric cancer cells in culture by reducing *FOXN3* and *RECK* mRNAs. Levels of these mRNA targets, which encode tumor suppressor, are reduced in human gastric tumors.

INTRODUCTION

Chronic inflammation and infection increase the risk of inflammation-induced gastrointestinal (GI) tumorigenesis[1, 2]. The secretion of pro-inflammatory cytokines and chemokines by infiltrated immune cells creates a pro-tumorigenic microenvironment that contributes to the malignant transformation of epithelial cells[3]. In epithelial cells, many genes are regulated by cytokines that activate transcription factors, such as STAT3 and NF-κB[4, 5]. Thus, investigating altered gene expression in epithelial cells in response to inflammatory signals is important to a comprehensive understanding of inflammation induced-carcinogenesis.

MicroRNAs (miRNAs) are an important class of gene expression regulators. They are small non-coding RNAs of 18-23 nucleotides involved in the post-transcriptional regulation of gene expression. They generally bind to the 3'-untranslated region (3'-UTR) of target transcripts and inhibit the gene expression by translational repression or transcript degradation[6]. Dysregulated miRNAs have been reported in inflammation, cancer development and progression by targeting genes that regulate proliferation, differentiation and apoptosis[7]. However, our understanding of the changes in miRNA expression during inflammation-induced carcinogenesis remains incomplete.

A key technical challenge in the cell type-specific study of miRNA *in vivo* is the heterogeneity in tissue microenvironment, a problem that is accentuated in an inflamed tumor infiltrated with immune cells. The presence of immune cells or stromal cells not only functionally affects the physiology of epithelial cells, but also masks the true expression pattern of miRNAs within epithelial cells[8-10]. Furthermore, recent studies have demonstrated that secreted miRNAs from the immune cells would impact on the gene expression in the

other cell types, including epithelial cells. As such, laser microdissection is well suited for cell type-enriched miRNA expression profiling as it preserves the complex cell-cell interaction within a heterogeneous tissue niche *in vivo* while negating the problem of mixed cell populations during measurement.

In this study, we undertake the profiling of epithelial-enriched miRNA in normal, inflamed or cancerous gastric tissues, with the aid of laser microdissection. Together with changes in other miRNA, a strong upregulation of microRNA 135b (*MIR135b*, also called miR-135b) was observed in gastric epithelial cells during gastric inflammation and carcinogenesis, which was confirmed by *in situ* hybridization. Moreover, miR-135b was strongly induced in all gastric epithelial cell types following infection with *Helicobacter felis*. Although aberrant miR-135b expression has been reported in several cancer types, its link with inflammation has yet to be established[11-13]. Here, we demonstrate that miR-135b acts downstream of IL-1β and promotes tumorigenic activities *in vitro* by targeting *FOXN3* and *RECK*. Clinically, persistent miR-135b expression is observed from early-stage gastric cancer and correlates inversely with *FOXN3* and *RECK* mRNA levels, supporting the clinical relevance of the IL-1-miR-135b signaling axis.

METHODS AND MATERIALS

Mouse models

Murine gastritis (K19-C2mE) and gastric tumor (K19-Wnt1/C2mE; Gan) models were generated as described previously[14, 15]. K19-C2mE mice express *Ptgs2* and *Ptges* in gastric mucosa, resulting in the development of inflammation-associated metaplastic hyperplasia caused by increased prostaglandin E_2 (PGE_2) levels. Gan mice express *Wnt1*, *Ptgs2* and *Ptges* in the stomach, which results in gastric tumor development caused by simultaneous activation

of Wnt signaling and COX-2/PGE_2 pathways.

Mice bearing *miR-135b-lacZ-neo*$^{fl/fl}$ were acquired from the Jackson Laboratory (Bar Harbor, ME, USA). The expression of miR-135b is disrupted in all tissues of homozygote *miR-135b-lacZ-neo* (*miR-135b-ln*$^{fl/fl}$) mice by the insertion of upstream polyA sequences at the end of *lacZ* and *neo* coding sequences (Supplementary Figure S1)[16]. In this study, we employed the *miR-135b-ln*$^{fl/fl}$ mouse as a non-tissue-specific conventional knockout without tissue-specific conditional deletion by Cre/loxP. The *miR-135b-ln*$^{fl/fl}$ mice were crossed with K19-C2mE or Gan, and examined at 40 to 50 weeks of age. Histological analyses and scoring of proliferation, metaplasia and inflammation of hyperplastic lesions were conducted as previously reported[17] and detailed in Supplementary Material. All animal experiments were conducted as approved by the Committee on Animal Experimentation of Kanazawa University, Japan.

Helicobacter felis infection of mouse stomachs

Helicobacter felis (*H. felis*; ATCC49179) was cultured as previously described[14] and inoculated at 10^8 CFU/mouse per oral administration (*p.o.*) into wild-type C57BL/6 mice. The infected mice were examined 8 weeks after the *H. felis* inoculation (n=4 each for uninfected control and *H. felis* infection).

In situ hybridization

Precursor miR-135b (pre-miR-135b) was detected by *in situ* hybridization using the BaseScope™ Assay with Detection Reagents-RED (Advanced Cell Diagnostics, Hayward, CA, USA; hereafter referred to as BaseScope), in accordance to the accompanied instructions. DapB was used as a negative control.

Epithelial cell-enriched microRNA expression profiling

Wild type (WT) and Gan mice tumors (n=4) were prepared as 10 μm frozen sections and stained with toluidine blue (Wako, Tokyo, Japan). Gastric epithelial cells were enriched by laser microdissection (LMD) on a LMD7000 laser microdissection system (Leica Microsystems, Wetzlar, Germany). RNA was purified with the MicroRNeasy Microkit (Qiagen GmbH, Hilden, Germany) and quantified on an Agilent 2100 Bioanalyzer (Agilent Technologies, Santa Clara, CA, USA). MicroRNA profiling was performed on the Agilent Mouse miRNA Microarray platform and analyzed with the GeneSpring GX software package (Agilent Technologies).

Organoid and cell culture experiments

Human gastric cancer (GC) cell lines SNU-719, SNU-601, SNU-638 and AGS were acquired from the Korean Cell Line Bank (Seoul, Korea) or ATCC (Manassas, VA, USA) and were cultured under recommended conditions. The immortalized gastric lines GIF-14 and its K-Ras^{G12V} expressing derivative were cultured as previously described[18]. For MEK inhibitors treatment, cells are treated with U0126 (10 μM; Tocris Bioscience, Bristol, UK); Trametinib (50 nM; Selleck, Houston, USA); PD98059 (10 μM; Tocris) and PD0325901 (1 μM; Sigma-Aldrich) or DMSO for 24 h. Gastric corpus organoids were grown from wild type and *miR-135b-ln*$^{fl/fl}$ C57BL/6 mice as previously reported[19] and detailed in Supplementary Materials. After 3 days, organoids were treated with 100 ng/ml of IL-1α (Wako), 100 ng/ml IL-1β (Wako), 100 ng/ml tumor necrosis factor-α (TNF-α; Wako), interferon-γ (IFN-γ; PeproTech), lipopolysaccharide (LPS; Wako) or peptidoglycan (PGN-SA; InvivoGen, San Diego, CA, USA) for the indicated duration.

Assays of stemness, tumorigenicity and cell migration

For sphere assays, GIF-14 cells were transfected with a miR-135b microRNA or an unrelated control double-stranded microRNA mimic (Thermo Fisher Scientific, Waltham, MA, USA)

before seeded on a 6-well ultra-low adherent plate (Corning, Corning, NY, USA) at a density of 2,500 cells per well as previously described[20]. Spheres were cultured for 2 weeks and counted. In soft agar colony formation assays, cells transfected with control or miR-135b mimic were mixed in 0.4% agar and cultured for the indicated time in a 6-well plate. Colonies were stained with Giemsa stain (Wako) and counted. For Transwell migration assay, cells were transfected with microRNA mimics, control or miR-135b inhibitor (TuD135, Sigma-Aldrich, St. Louis, MO, USA) and seeded in the upper chamber. The migrated cells were stained with Calcein AM (Corning) after 12 to 24 hours and counted. For functional validation by migration assays, 30 nM of siFOXN3 or siRECK (Ambion) were transiently transfected into SNU-638 cells.

Analysis of human gastric tumor samples

Twenty-eight pairs of human GC and corresponding normal mucosa (NM) tissues were obtained from Kanazawa University Hospital (Kanazawa, Ishikawa, Japan) as previously described[21]. This study has been approved by the Kanazawa University Medical Ethics Committee and written informed consent was obtained prior to specimen collection[21]. Publicly available, level 3 data of The Cancer Genome Atlas (TCGA) were analyzed in the current study. Clinical information and miRNA expression data of the TCGA samples were downloaded from the USCS Cancer Browser (https://genome-cancer.ucsc.edu). The patients' clinical data and molecular subtype status of stomach cancer were referred from the TCGA database[22]. Among TCGA stomach cancer cohort, 436 tumor and 41 normal stomach samples that included miR-135b expression data were analyzed for the current study. The reads per kilobase of exon per million reads mapped (RPKM) value was used to represent the expression level of genes.

RNA extraction and quantitative real-time RT-PCR for miRNA and mRNA

Total RNA were extracted using the miRNeasy Microkit (Qiagen) or the ISOGENII reagent (Nippon Gene; Toyama, Japan). MicroRNAs and mRNA expression were quantified by TaqMan miRNA assays (Applied Biosystems, Foster City, CA, USA) or with SYBR Premix ExTaqII (Takara, Kusatsu, Japan) using gene specific oligonucleotide primers (Supplementary Table S1) on a Stratagene Mx3000P QPCR Systems (Agilent Technologies). The expression levels of U6 or snoRNA202 miRNA, and *GAPDH* or *ACTB* mRNA, were used to normalize the expression levels of miR-135b and its mRNA targets, respectively.

Luciferase reporter assays

The 3'-UTR of *FOXN3* and *RECK* were amplified (Supplementary Table S1) and cloned into pmirGLO Dual Luciferase reporter vector (Promega, Madison, WI, USA). These vectors were checked by capillary sequencing and transiently transfected into SNU-638 cells together with control or miR-135b mimic microRNAs. Cells were harvested 24h post transfection and assayed for firefly luciferase and *Renilla* luciferase activities on a Centro XS^3 LB960 luminometer (Berthold Technologies, Bad Wildbad, Germany).

Statistical analysis

All data were presented as the mean ± standard deviation (SD), except otherwise indicated. Paired t-test, student t-test and Kruskal-Wallis tests were performed to analyze miRNA and mRNA expression. Pearson's correlation analysis was used to compare between miR-135b and target genes expression. The *p* values were indicated on the figures as follows: *, $p<0.05$; **, $p<0.01$; ***, $p<0.001$. These statistical results were generated using the GraphPad Prism V5.0 software package (GraphPad Software, La Jolla, CA, USA). For analysis of TCGA datasets, Wilcoxon rank sum analysis was performed to analyze the expression levels of miR-135b with respect to cancer stages, and Tukey post-hoc ANOVA was performed for the comparison across gastric cancers of different molecular subtypes.

RESULTS

Identification of inflammation-induced miRNAs in gastric carcinoma cells

In a previous study, the miRNA expression in the gastric lesions of gastritis mouse model (K19-C2mE) and gastric tumor model (Gan) were profiled, from which inflammation- and tumor-associated miRNAs were identified[21]. These expression patterns consisted of miRNAs from epithelial cells, stromal cells and leukocytes within the tissue microenvironment[21]. To reduce the contribution from non-epithelial cells, Laser Microdissection (LMD) was employed to enrich epithelial cells from normal and gastric tumor samples prior to miRNA microarray analyses (Figure 1A). This revealed the up-regulation of 100 miRNAs (≥ 2.0-fold; $p<0.05$) and down-regulation of 40 miRNAs (≤ 0.5-fold; $p<0.05$) in Gan mouse gastric tumor epithelial cells relative to normal epithelial cells (Figure 1B; Supplementary Table S2). To strengthen these observations, this epithelial-enriched miRNA profiles were integrated with profiles previously established from mixed cell populations[21], using the GeneSpring GX software package. This identified 18 miRNAs whose expression levels were upregulated and 12 miRNAs downregulated in an inflammation-dependent manner in enriched tumor epithelial cells (Figure 1C; Supplementary Table S3). Of these, miR-135b was the most highly induced miRNAs in the epithelial cells of both the K19-C2mE gastritis and Gan gastric cancer models.

To confirm this observation, LMD enrichment of epithelial cells was repeated on K19-C2mE gastritis lesions and Gan gastric tumors, and strong elevation of miR-135b expression was similarly observed, compared with those collected from wild type stomachs (Figure 1D). Interestingly, there was no significant difference between the miR-135b expression levels in K19-C2mE gastritis lesions and Gan tumors (Figure 1D and Supplementary Figure S2). As the Gan mice also bear the K19-C2mE transgenes (*Ptgs2* and

Ptges) in addition to *Wnt1*, this observation associates the induction of miR-135b with the gastric inflammation driven by COX-2/PGE_2 pathway[14, 23]. To further confirm the epithelial-specific expression of miR-135b, we performed *in situ* hybridization of pre-miR-135b using the BaseScope assay. This revealed an epithelial-specific expression pattern that was greatly increased in K19-C2mE gastritis lesions and Gan gastric tumors in association with increased cellular proliferation (Figure 1E). Lastly, we performed LMD enrichment of epithelial cells in the gastric tumors that spontaneously develop in $gp130^{F/F}$ mice, an independent model of inflammation-induced gastric carcinogenesis[24]. This revealed that miR-135b is also strongly over-expressed in $gp130^{F/F}$ tumor cells, providing further support that elevated miR-135b expression is associated with gastric inflammation and gastritis-associated carcinogenesis (Figure 1F).

The upregulation of miR-135b is an early event in gastric carcinogenesis

To better understand the kinetics of miR-135b induction during Gan gastric tumorigenesis, we applied LMD to extract gastric tumor cells and their matched normal counterparts from young (<8 weeks old) and old (50 weeks) Gan mouse stomachs. This revealed a strong increase of miR-135b expression even in the early gastric lesions of young Gan mice, which was not further increased in older mice. This suggests that miR-135b induction occurs early during Gan carcinogenesis (Figure 2A).

We next extended this investigation to clinical samples, where the expression of miR-135b was examined in 28 pairs of human gastric cancers (GC) and matched normal mucosa samples. Quantitative RT-PCR analyses showed that miR-135b expression was significantly higher in the GC samples compared with their matched normal counterparts (Figure 2B). Moreover, miR-135b levels were found significantly elevated in early stage (Stages I/II) as well as in advanced (Stages III/IV) GC samples, with no significant difference

between early and advanced stage samples (Figure 2C). These observations are supported by data derived from stomach adenocarcinoma patients deposited in The Cancer Genome Atlas (TCGA) repository[22], wherein miR-135b levels are significantly elevated in GC samples of all stages ($p<0.001$; Figures 2D and 2E). Notably, miR-135b expression is elevated in GC samples from the earliest T1 Stage and Stage I and is consistently maintained through more advanced stages. Interestingly, when grouped according to the molecular subtypes published by the TCGA[22], miR-135b levels are significantly lower in GC samples classified as genomically stable, compared with other subtypes ($p<0.001$; Figure 2F). Overall, our analyses revealed increases in miR-135b expression in pre-cancerous mouse tissues and early stages of human GI tumors, which were maintained during disease progression, indicating that the upregulation of miR-135b is an early event in gastric carcinogenesis.

MiR-135b mediates gastric inflammation downstream of the IL-1β /MyD88 axis

Given the strong increase in miR-135b observed during gastritis, we sought to identify the pro-inflammatory signals responsible. Wild-type mouse gastric organoids were treated with pro-inflammatory cytokines (IL-1α, IL-1β, TNF-α) previously reported to promote K19-C2mE gastritis or Gan tumorigenesis[25, 26] and pathogen-associated molecular pattern (PAMP) molecules, namely LPS (TLR4 ligand) or PGN-SA (TLR2 ligand). Significant induction of miR-135b expression was observed over time in IL-1α and IL-1β treated organoids (Figure 3A and 3B). We also examined the effects of IFN-γ, which plays a role in gastric metaplasia[27, 28] and found that it displayed cytotoxicity on gastric organoids at concentrations above 0.5ng/ml (Supplementary Figure S3A). However, it had little or no effect on miR-135b expression at the non-toxic dose of 0.5ng/ml, in contrast with IL-1β (Supplementary Figure S3B and Fig. 3B). In addition to gastric organoids, IL-1β-responsiveness of miR-135b was observed in an immortalized fetal gastric epithelial cell line,

GIF-14[29] (Figure 3C). Collectively, these observations suggest that IL-1 signaling is a major driver of miR-135b expression in gastric epithelial cells during inflammation.

Two well-characterized downstream events of IL-1/MyD88 signaling are the activation of the NF-κB and MAPK pathways. The inability of TNF-α and TLR agonists, potent activators of the NF-κB pathway, to induce miR-135b indicate the utilization of MAPK pathway. To investigate the involvement of MAPK pathway in the regulation of miR-135b, we treated GIF-14 K-Ras^{G12V} cells, in which the MEK/ERK pathway is constitutively active, with an MEK1/2 inhibitor, U0126. This resulted in significant suppression of miR-135b expression (Figure 3D), suggesting that IL-1α and -β induced miR-135b via the MAPK pathway. Due to the general toxicity of MEK inhibitors on gastric organoids (Supplementary Figure S4) we could not readily evaluate their effects on miR-135b expression. Therefore, we repeated the experiment on SNU-601 cells that have high basal expression of miR-135b and found that miR-135b level is significantly attenuated by four separate MEK1/2 inhibitors (Figure 3E). To understand how MEK may regulate miR-135b, we queried the ENCODE Project ChIP-Seq data, which revealed the binding of JUND and ATF2 to the miR-135b proximal promoter (Supplementary Figure S5). These transcription factors are known mediators of several signalling pathways, including MAPK/MEK. Taken together, our observations support the involvement of MAPK downstream of IL-1β in driving miR-135b expression.

We next measured the expression of *Il1b* in whole K19-C2mE and Gan mouse tissues and observed that *Il1b* expression was significantly elevated, compared with wild-type stomach (Figure 4A). Moreover, *Il1b* levels were strongly correlated with those of miR-135b ($r=0.759$, $p<0.0001$; Figure 4B). To investigate the source of IL-1β that fuels miR-135b expression *in vivo*, epithelial and stromal cells were enriched by LMD from normal or Gan mouse tissues. This revealed that relative to normal or cancerous epithelial cells, the

expression of *Il1b* is much higher in the stromal cells within the Gan tumor tissues (Figure 4C). This suggests that the strong increase in miR-135b in gastric epithelial cells during inflammation is driven at least in part by stromal cell-derived IL-1β.

To further assess the contribution of IL-1 signaling, we generated Gan mice deficient in Myd88, a key adaptor protein of IL-1R1 requisite for downstream signaling. *Myd88*$^{-/-}$ Gan mice developed much smaller gastric adenocarcinomas[26]. Notably, the expression of miR-135b was greatly reduced in *Myd88*$^{-/-}$ Gan tumors, compared with *Myd88*$^{+/+}$ Gan tumors (Figure 4D). Although it is possible that this was an indirect effect of the reduced pathologies of the *Myd88*$^{-/-}$ Gan tumors, this observation is consistent with miR-135b acting downstream of the IL-1/MyD88 signaling axis during gastritis-associated tumorigenesis.

To determine the role of miR-135b in the etiologies of gastritis-associated carcinogenesis *in vivo*, we introduced the *miR-135b-ln*^{fl} allele that disrupts miR-135b expression into the K19-C2mE gastritis mice. K19-C2mE mice develop metaplastic hyperplasia in the stomach caused by COX-2 and mPGES-1 expression, with features similar to precancerous spasmolytic polypeptide-expressing metaplasia (SPEM)[14, 15]. Notably, the disruption of *Mir135b* significantly suppressed the gastric hyperplasia in K19-C2mE mice (Fig. 4E-4H). Mean lesion size of *miR-135b-ln*$^{fl/fl}$ K19-C2mE mice was reduced by ~50% compared with *miR-135b*$^{wt/wt}$ K19-C2mE mice (Figure 4F and 4G). Concordantly, Ki67 labeling index was significantly decreased in *miR-135b-ln*$^{fl/fl}$ K19-C2mE mice (Figure 4F and 4H). In contrast, the severity of metaplasia and inflammation was not changed by suppression of miR-135b expression (Supplementary Figure S6). Interestingly, miR-135b-deficiency did not affect organoids generation and growth under standard *ex vivo* culture conditions, possibly due to the lack of inflammatory cues, or that miR-135b deficiency was compensated by the supplemented growth factors (Supplementary Figure S7).

We next assessed the potential contribution for miR-135b in tumorigenesis by generating compound *miR-135b-ln*$^{fl/fl}$ Gan mice. However, the disruption of miR-135b did not significantly reduce tumor sizes (Supplementary Figure S8), suggesting that miR-135b is dispensable for tumorigenesis when Wnt signaling is sufficiently activated. Lastly, we infected wild-type mice with *H. felis* to induce gastric inflammation[14]. Eight weeks post-infection, we observed inflammatory infiltration and a profound induction of miR-135b expression by BaseScope *in situ* hybridization (Figure 4I and Supplementary Figure S9), hence providing an important link between miR-135b induction and pathogen-induced inflammation. Furthermore, we confirm by Ki-67 staining that *H. felis*-induced gastritis is associated with increased epithelial cell proliferation (Figure 4J). Collectively, these observations indicate that miR-135b is part of an innate epithelial-specific response to infection and inflammation that plays an important role in the early, pre-neoplastic stages of gastric carcinogenesis.

miR-135b promotes tumorigenic and stem-like properties in vitro

Having established a role for miR-135b in gastric inflammation *in vivo*, we sought to determine the cellular functions of miR-135b. Double-stranded miR-135b mimic RNA (miR-135b mimic) or single-stranded miR-135b-targeting inhibitors (miR-135b inhibitor) were transfected into a series of gastric carcinoma lines. In soft agar assays, miR-135b mimic significantly increased the ability of AGS, SNU638 and SNU-719 gastric carcinoma cells to grow in an anchorage-independent manner, reflecting an increase in tumorigenicity (Figure 5A). Consistently with this, in Transwell cell migration assays, miR-135b mimic significantly increased cell migration in SNU-638 gastric carcinoma cells and GIF-14 immortalized gastric epithelial cells, both of which have low endogenous miR-135b expression (Figure 5B). Conversely, miR-135b inhibitor caused the strongest reduction in cell migration in gastric

lines with high endogenous miR-135b expression, most notably SNU-601 (Figure 5B). To investigate if miR-135b induces greater stem-like properties and cellular plasticity, sphere assays were conducted using GIF-14 gastric epithelial cells, an established *in vitro* model of cellular plasticity and stemness[8, 20]. The introduction of miR-135b mimic significantly increased the ability of GIF-14 cells to form spheres in serum-free culture, suggesting that it promotes stem-like properties and cellular plasticity in gastric epithelial cells (Figure 5C).

miR-135b mediates its functions by directly targeting FOXN3 and RECK

To understand how miR-135b may mediate its oncogenic effects, an *in silico* analysis was conducted to identify putative target genes of miR-135b in gastric epithelial cell. Firstly, utilizing three independent target gene prediction programs (TargetScan7.1, StarBase2.0 and microRNA.org), 633 common predicted target genes were identified. Of these, 104 genes were down-regulated in either the K19-C2mE or Gan mice expression datasets, and 275 genes were shared with those down-regulated in the human gastric tumors analyzed in this study and in the TCGA human adenocarcinoma data repository (Figure 6A). Notably, a restricted subset of 21 predicted target genes were found under-represented in the human and mouse tissues profiled (Figure 6A). A functional annotation analysis (https://david.ncifcrf.gov/; Supplementary Table S4) was performed on the 21 short-listed candidates. This analysis suggested that *FOXN3* (forkhead box N3) and *RECK* (reversion-inducing cysteine-rich protein with kazal motifs) mRNAs are potential physiological targets of miR-135b in gastric epithelial cells (Figure 6A).

To determine if *FOXN3* or *RECK* mRNAs are authentic targets of miR-135b, we generated reporter gene constructs wherein the 3'-UTR sequences of *FOXN3* or *RECK* were fused with the firefly luciferase coding sequence (Figure 6B). In transient transfection studies performed in SNU-638 gastric carcinoma cells and HEK293T cells, the introduction of

FOXN3 and *RECK* 3'-UTRs significantly suppressed reporter activities when cells were co-transfected with miR-135b mimic (Figure 6C and 6D, and Supplementary Figure S10). Sequence analyses with TargetScan 7.1 software identified two miR-135b target sites within the *FOXN3* 3'-UTR that are conserved between mouse and human. To evaluate their functionality, these sites were mutated individually or in combination (Figure 6B). In co-transfection assays, the mutation of each of these sites partially abrogated the effects of miR-135b mimic, while their concurrent mutation fully blocked miR-135b-mediated attenuation of luciferase activity (Figure 6C and Supplementary Figure S10). In the case of *RECK* mRNA, a single conserved miR-135b site was identified in the 3'-UTR and its mutation was able to protect the reporter mRNA from targeting by the miR-135b mimic (Figure 6B and 6D, and Supplementary Figure S10).

To investigate the cellular functions of *FOXN3* and *RECK*, we performed Transwell migration assay after transfecting siRNAs against *FOXN3* or *RECK* in SNU-638 gastric carcinoma cells. This showed that the RNAi targeting of *FOXN3* and *RECK* significantly enhanced cell migration to levels comparable to that of miR-135b, in a manner independent of cell proliferation (Figure 6E and Supplementary Figure S11). Interestingly, a comparison of *Foxn3* and *Reck* expression levels in wild type, K19-C2mE and Gan mouse stomach tissues revealed two distinct patterns. *Foxn3* expression was significantly decreased in the K19-C2mE gastritis, but not in the Gan tumor tissues (Figure 6F). In contrast, *Reck* expression was strongly suppressed in both gastritis and tumor tissues (Figure 6F). This difference indicates that miR-135b is only partially responsible for the overall regulation of *Foxn3*, which is likely to be also regulated by the constitutively active Wnt signaling in Gan mouse. Nevertheless, the expression levels of both *Foxn3* and *Reck* mRNAs are inversely correlated to miR-135b to statistical significance in these tissues samples (Figure 6F). Moreover, the expression of *Foxn3* and *Reck* are inversely correlated with *Il1b* levels in these

tissues, further indicating that miR-135b acts downstream of IL-1β to suppress *Foxn3* and *Reck* mRNAs (Supplementary Figure S12). Lastly, we queried the TCGA database and confirmed that *FOXN3* and *RECK* mRNA expression are strongly and inversely correlated with miR-135b in human gastric cancer tissues (Figure 6G). Together, these data provide compelling evidence that miR-135b mediates its pro-inflammatory and tumor promoting activity in part by inhibiting *FOXN3* and *RECK* expression, two target genes with known tumor suppressor functions.

DISCUSSION

MicroRNAs play a major role in the modulation of gene expression and the maintenance of homeostasis. During carcinogenesis, miRNAs often act as downstream effectors of key oncogenic pathways to activate or repress transcriptomic programs. However, attempts to identify these oncogenic miRNAs are often hampered by the heterogeneous nature of the tumor and its microenvironment[30, 31]. Altered miRNA expression during the transformation of epithelial cells could potentially be masked by changes in tissue composition resultant from structural disruption and inflammation. For the same reason, whole tissue gene expression profiling is prone to false positives. To resolve this problem, we employed laser microdissection to enrich gastric epithelial cells and interrogate changes in miRNA expression during inflammation-associated carcinogenesis. Using gastric tissues from the K19-C2mE gastritis and Gan stomach tumor mouse models, we identified a strong epithelial-specific induction of miR-135b during chronic inflammation that was also observed in Gan carcinoma cells. Moreover, several cancer-associated miRNAs previously identified as over-expressed through mixed population gene expression profiling, such as miR-18a and miR-130b, are absent in our dataset[21, 32]. These observations highlight the utility of our approach

in deconvoluting the complex contribution of the altered miRNA transcriptome within the tumor microenvironment. Furthermore, the fidelity of this LMD-assisted approach was supported by BaseScope *in situ* hybridization, which revealed clear epithelial-specific expression and induction of miR-135b in gastric epithelial cells in K19-C2mE and Gan tissues, and during *H. felis* infection.

Our data are consistent with miR-135b functioning as an important downstream effector of gastric inflammation in gastric epithelial cells. The expression of miR-135b was previously reported to be under the regulation of a range of extracellular stimuli, including the canonical Wnt, PTEN/PI3K, Hippo and c-Src pathways[12]. Using organoid cultures, we demonstrate that the proinflammatory signal that drives miR-135b expression in normal gastric epithelial cells comes from IL-1. Curiously, TNF-α does not appear to contribute to miR-135b expression in this context, which suggests IL-1 exerts its effect via its MAPK/ERK signaling axis. In support of this, the pharmacological inhibition of MEK1/2 significantly suppressed miR-135b expression in immortalized gastric epithelial cells expressing oncogenic K-Ras and in SNU-601 cells, a gastric carcinoma line bearing the $KRAS^{G12D}$ mutation. As promoter polymorphisms in *IL1B* are associated with both chronic atrophic gastritis and gastric cancers, we investigated the correlation between *IL-1β* and miR-135b levels in mouse and human gastric tissues[33, 34]. This revealed a tight correlation between the expression of IL-1β and miR-135b in mouse and human tumor tissues. In addition to gastric cancer, IL-1β is genetically or functionally linked to inflammation-induced cancers in diverse tissues[35]. Importantly, miR-135b has been implicated in many of these cancers[12, 36-38]. As such, the findings of this study may facilitate our understanding of miR-135b as a mediator downstream of IL-1β-driven inflammation and carcinogenesis beyond the gastric epithelium.

To understand how miR-135b serves its role, we surveyed putative target genes that might confer greater resilience against injury while enhancing proliferation in a remodeling

and inflamed tissue microenvironment. This led to the identification of two important target genes with tumor suppressor activities, *FOXN3* and *RECK*. FOXN3 is a Forkhead-related transcription factor that acts as a negative regulator of cellular proliferation, notably during DNA damage[39]. In addition, FOXN3 suppresses cell proliferation by being a transcriptional repressor of E2F5[40] and safeguards against aberrant epithelial-mesenchymal transition (EMT)[38]. With these multi-modal tumor suppressor activities, it is unsurprising that FOXN3 expression is reduced in diverse cancer types[41]. In the context of this study, the targeting of *FOXN3* mRNA by miRNA-135b is likely part of an epithelial-specific transcriptomic program that affords epithelial cells greater resilience and regenerative proliferation during inflammation, infection and injury[14].

Similarly, *RECK* is downregulated in many types of cancer though its tumor suppressor activities are distinct from those of FOXN3. RECK is a membrane-bound inhibitor of several membrane-type metalloproteinases, in particular MT1-MMP, and is a potent negative regulator of cell motility[42, 43]. RECK is also a key player in vascularization and is important to cell migration during normal development[42]. In cancer, the loss of *RECK* is associated with increased tumor vascularization and EMT of tumor cells[44]. Taken together, the targeting of *RECK* by miR-135b supports a role for miRNA-135b in tissue remodeling and wound healing as per normal EMT[45, 46]. Interestingly, the knockdown of *FOXN3* and *RECK* did not alter cellular proliferation in our in vitro studies, indicating that other miR-135b targets may be involved, or that the mitogenic activities of FOXN3 and RECK were masked by the dominant driver mutations in the gastric cancer cells, concordant with the observations in the Gan mouse model. Instead, miR-135b promoted cellular migration, implicating a further role in supporting tumor progression and metastasis. Although the mouse models used in this study do not progress to metastatic malignancies, these

observations may explain the sustained over-expression of miR-135b in advance human gastric cancers.

The K19-C2mE transgenic mouse model spontaneously develops gastric inflammation, metaplasia and dysplasia, with heavy infiltration of macrophages, due to epithelial expression of ectopic COX-2 and mPGES-1[14, 23, 47]. In the Gan mouse model, ectopic Wnt1 was introduced in addition to COX-2 and mPGES-1 to further model stepwise carcinogenesis in an inflamed stomach[15]. This resulted in strong tumorigenicity in the glandular stomach, coupled with heightened discharge of ROS due to tissue damage[15, 25, 48]. Here, we observed that miR-135b is strongly induced in K19-C2mE gastritis and early during Gan tumorigenesis. Interestingly, miR-135b levels were not significantly different between K19-C2mE and Gan gastric tissues, suggesting that miR-135b acts primarily downstream of gastritis to generate a pre-malignant hyperplastic state from which a strong oncogenic signal could drive tumorigenesis. This process appears to be dependent on an inflamed tissue microenvironment, as miR-135b deficiency had no apparent effects on organoid growth in *ex vivo* culture but significantly reduced gastritis-associated hyperplasia *in vivo.* An early role for miR-135b is also supported by the increased miR-135b expression observed at the earliest clinical stages during human gastric carcinogenesis. This is functionally demonstrated in the observation that miR-135b-deficiency could effectively attenuate the gastritis-associated hyperproliferation in K19-C2mE mice but had no discernible effect on Gan tumorigenesis, where its contribution is overshadowed by the dominant effects of Wnt signaling.

Finally, despite great advances in our understanding of the pathogenesis, etiology and the genomics of gastric cancer, it remains the third most lethal cancer worldwide, often due to its late detection. Therefore, there is an urgent need for better diagnostics. Encouragingly, miR-135b could be readily detected in the culture supernatant of over-expressing cells (Supplementary Figure S13). This property, coupled with the association of miR-135b with

gastritis and early-stage gastric carcinogenesis suggest miR-135b may find utility in the development of diagnostic tools for the early detection of gastric abnormalities.

Acknowledgments

The authors are grateful to Manami Watanabe, Ayako Tsuda and Yoshie Jomen for their technical assistance.

REFERENCES

1. Fox JG, Wang TC. Inflammation, atrophy, and gastric cancer. J Clin Invest 2007;117:60-9.
2. Terzic J, Grivennikov S, Karin E, et al. Inflammation and colon cancer. Gastroenterology 2010;138:2101-2114 e5.
3. Coussens LM, Werb Z. Inflammation and cancer. Nature 2002;420:860-7.
4. Zhong Z, Wen Z, Darnell JE, Jr. Stat3: a STAT family member activated by tyrosine phosphorylation in response to epidermal growth factor and interleukin-6. Science 1994;264:95-8.
5. Keates S, Hitti YS, Upton M, et al. Helicobacter pylori infection activates NF-kappa B in gastric epithelial cells. Gastroenterology 1997;113:1099-109.
6. Ha M, Kim VN. Regulation of microRNA biogenesis. Nat Rev Mol Cell Biol 2014;15:509-24.
7. Lin S, Gregory RI. MicroRNA biogenesis pathways in cancer. Nat Rev Cancer 2015;15:321-33.
8. Baltimore D, Boldin MP, O'Connell RM, et al. MicroRNAs: new regulators of immune cell development and function. Nat Immunol 2008;9:839-45.
9. O'Connell RM, Rao DS, Chaudhuri AA, et al. Physiological and pathological roles for microRNAs in the immune system. Nat Rev Immunol 2010;10:111-22.
10. **Rodriguez A**, **Vigorito E**, Clare S, et al. Requirement of bic/microRNA-155 for normal immune function. Science 2007;316:608-11.
11. **Matsuyama H**, **Suzuki HI,** Nishimori H, et al. miR-135b mediates NPM-ALK-driven oncogenicity and renders IL-17-producing immunophenotype to anaplastic large cell lymphoma. Blood 2011;118:6881-92.
12. Valeri N, Braconi C, Gasparini P, et al. MicroRNA-135b promotes cancer progression by acting as a downstream effector of oncogenic pathways in colon cancer. Cancer Cell 2014;25:469-83.
13. Lin CW, Chang YL, Chang YC, et al. MicroRNA-135b promotes lung cancer metastasis by regulating multiple targets in the Hippo pathway and LZTS1. Nat Commun 2013;4:1877.

14. Oshima H, Oshima M, Inaba K, et al. Hyperplastic gastric tumors induced by activated macrophages in COX-2/mPGES-1 transgenic mice. Embo j 2004;23:1669-78.

15. Oshima H, Matsunaga A, Fujimura T, et al. Carcinogenesis in mouse stomach by simultaneous activation of the Wnt signaling and prostaglandin E2 pathway. Gastroenterology 2006;131:1086-95.

16. Park CY, Jeker LT, Carver-Moore K, et al. A resource for the conditional ablation of microRNAs in the mouse. Cell Rep 2012;1:385-91.

17. Rogers AB. Histologic scoring of gastritis and gastric cancer in mouse models. Methods Mol Biol 2012;921:189-203.

18. **Voon DC**, **Wang H**, Koo JK, et al. EMT-induced stemness and tumorigenicity are fueled by the EGFR/Ras pathway. PLoS One 2013;8:e70427.

19. **Barker N**, **Huch M**, Kujala P, et al. Lgr5(+ve) stem cells drive self-renewal in the stomach and build long-lived gastric units in vitro. Cell Stem Cell 2010;6:25-36.

20. **Voon DC**, **Wang H**, Koo JK, et al. Runx3 protects gastric epithelial cells against epithelial-mesenchymal transition-induced cellular plasticity and tumorigenicity. Stem Cells 2012;30:2088-99.

21. **Kong D**, **Piao YS**, Yamashita S, et al. Inflammation-induced repression of tumor suppressor miR-7 in gastric tumor cells. Oncogene 2012;31:3949-60.

22. The Cancer Genome Atlas Research Network. Comprehensive molecular characterization of gastric adenocarcinoma. Nature 2014;513:202-9.

23. Oshima H, Hioki K, Popivanova BK, et al. Prostaglandin E(2) signaling and bacterial infection recruit tumor-promoting macrophages to mouse gastric tumors. Gastroenterology 2011;140:596-607.e7.

24. Jenkins BJ, Grail D, Nheu T, et al. Hyperactivation of Stat3 in gp130 mutant mice promotes gastric hyperproliferation and desensitizes TGF-beta signaling. Nat Med 2005;11:845-52.

25. **Oshima H**, **Ishikawa T**, Yoshida GJ, et al. TNF-alpha/TNFR1 signaling promotes gastric tumorigenesis through induction of Noxo1 and Gna14 in tumor cells. Oncogene 2014;33:3820-9.

26. Maeda Y, Echizen K, Oshima H, et al. Myeloid Differentiation Factor 88 Signaling in Bone Marrow-Derived Cells Promotes Gastric Tumorigenesis by Generation of Inflammatory Microenvironment. Cancer Prev Res (Phila) 2016;9:253-63.

27. Syu LJ, El-Zaatari M, Eaton KA, et al. Transgenic expression of interferon-gamma in mouse stomach leads to inflammation, metaplasia, and dysplasia. Am J Pathol 2012;181:2114-25.

28. Liu Z, Demitrack ES, Keeley TM, et al. IFNgamma contributes to the development of gastric epithelial cell metaplasia in Huntingtin interacting protein 1 related (Hip1r)-deficient mice. Lab Invest 2012;92:1045-57.

29. Fukamachi H, Mimata A, Tanaka I, et al. In vitro differentiation of Runx3-/- p53-/- gastric epithelial cells into intestinal type cells. Cancer Sci 2008;99:671-6.

30. **Han TS**, **Hur K**, Xu G, et al. MicroRNA-29c mediates initiation of gastric carcinogenesis by directly targeting ITGB1. Gut 2015;64:203-14.

31. Katada T, Ishiguro H, Kuwabara Y, et al. microRNA expression profile in undifferentiated gastric cancer. Int J Oncol 2009;34:537-42.

32. Yao Y, Suo AL, Li ZF, et al. MicroRNA profiling of human gastric cancer. Mol Med Rep 2009;2:963-70.

33. El-Omar EM, Carrington M, Chow WH, et al. Interleukin-1 polymorphisms associated with increased risk of gastric cancer. Nature 2000;404:398-402.

34. Machado JC, Pharoah P, Sousa S, et al. Interleukin 1B and interleukin 1RN polymorphisms are associated with increased risk of gastric carcinoma. Gastroenterology 2001;121:823-9.

35. **Xu J**, **Yin Z**, Cao S, et al. Systematic review and meta-analysis on the association between IL-1B polymorphisms and cancer risk. PLoS One 2013;8:e63654.

36. **Li Y**, **Xu D**, **Bao C**, et al. MicroRNA-135b, a HSF1 target, promotes tumor invasion and metastasis by regulating RECK and EVI5 in hepatocellular carcinoma. Oncotarget 2015;6:2421-33.

37. Nezu Y, Hagiwara K, Yamamoto Y, et al. miR-135b, a key regulator of malignancy, is linked to poor prognosis in human myxoid liposarcoma. Oncogene 2016.

38. **Mudduluru G**, **Abba M**, **Batliner J**, et al. A Systematic Approach to Defining the microRNA Landscape in Metastasis. Cancer Res 2015;75:3010-9.

39. Pati D, Keller C, Groudine M, et al. Reconstitution of a MEC1-independent checkpoint in yeast by expression of a novel human fork head cDNA. Mol Cell Biol 1997;17:3037-46.

40. **Sun J**, **Li H**, Huo Q, et al. The transcription factor FOXN3 inhibits cell proliferation by downregulating E2F5 expression in hepatocellular carcinoma cells. Oncotarget 2016;7:43534-43545.

41. **Huot G**, **Vernier M**, Bourdeau V, et al. CHES1/FOXN3 regulates cell proliferation by repressing PIM2 and protein biosynthesis. Mol Biol Cell 2014;25:554-65.

42. Oh J, Takahashi R, Kondo S, et al. The membrane-anchored MMP inhibitor RECK is a key regulator of extracellular matrix integrity and angiogenesis. Cell 2001;107:789-800.

43. Takahashi C, Sheng Z, Horan TP, et al. Regulation of matrix metalloproteinase-9 and inhibition of tumor invasion by the membrane-anchored glycoprotein RECK. Proc Natl Acad Sci U S A 1998;95:13221-6.

44. Mahl C, Egea V, Megens RT, et al. RECK (reversion-inducing cysteine-rich protein with Kazal motifs) regulates migration, differentiation and Wnt/beta-catenin signaling in human mesenchymal stem cells. Cell Mol Life Sci 2016;73:1489-501.

45. Gurtner GC, Werner S, Barrandon Y, et al. Wound repair and regeneration. Nature 2008;453:314-21.

46. **Nieto MA**, **Huang RY**, **Jackson RA**, et al. EMT: 2016. Cell 2016;166:21-45.

47. **Oguma K**, **Oshima H**, Aoki M, et al. Activated macrophages promote Wnt signalling through tumour necrosis factor-alpha in gastric tumour cells. Embo j 2008;27:1671-81.

48. Ishimoto T, Nagano O, Yae T, et al. CD44 variant regulates redox status in cancer cells by stabilizing the xCT subunit of system xc(-) and thereby promotes tumor growth. Cancer Cell 2011;19:387-400.

Author names in bold designate shared co-first authorship

FIGURE LEGENDS

Figure 1. *Discovery of inflammation-induced miRNAs in gastric tumor cells.* (A) The experimental approach utilized to identify tumor epithelial cell-specific microRNAs (miRNAs). Using the laser microdissection (LMD), epithelial cells were enriched and analyzed. (B) Results of miRNA microarray. Upregulated (≥2.0 fold) and downregulated (≤0.5 fold) miRNAs are presented as a bar graph. (C) Venn diagrams depicting the results of an integrated analysis that revealed upregulated (left) and downregulated (right) tumor epithelial-specific miRNAs (red), and those aberrantly expressed in inflamed (blue) and tumor (green) tissues of mixed populations. Upregulated (left) and downregulated (right) miRNAs are listed in descending and ascending expression levels, respectively. In tumor epithelial cells, miR-135b was the most upregulated miRNA by inflammatory response dependent manner. (D) Validation result of miR-135b in gastritis and gastric tumor epithelial cells. (E) Representative photographs of H&E staining (left), Ki-67 immunostaining (center), and *in situ* hybridization (BaseScope) detection of miR-135b (right), performed on wild-type stomach (top), K19-C2mE gastritis (middle), and Gan gastric tumor (bottom) tissues. Inserts indicate enlarged images of boxed region. Arrowheads indicate BaseScope positivity. Bars indicate 100 μm. (F) miR-135b expression levels in wild type (WT) stomach and $gp130^{F/F}$ gastric tumor epithelial cells, as measured by LMD-assisted qRT-PCR.

Figure 2. *Upregulation of miR-135b is an early event in gastric carcinogenesis.* (A) Laser microdissection (LMD) was used for enriching normal and tumor epithelial cells in the stomach of young (<8 weeks old) and 50-week old Gan mice (left). The expression of miR-135b (log_{10}) was measured by qRT-PCR (right). (B) The level of miR-135b expression (log_2) in human gastric cancer tissues relative to matched normal counterparts. (C) The expression

levels of miR-135b in 28 pairs of early (Stage I, II) and advanced (Stage III, IV) human gastric cancer (GC) and their matched normal mucosa (NM) tissues. (D, E, F) The expression of miR-135b in human gastric adenocarcinomas of different clinical stages and classifications. Expression data were extracted from the TCGA repository and charted in accordance to the T (D) and TNM (E) classifications of gastric cancer staging, and molecular subtypes (F). RPKM, reads per kilobase per million reads mapped; CIN, chromosomal instability; EBV, Epstein-Barr virus; GS, genomically stable; MSI, microsatellite instability.

Figure 3. *Inflammatory and mitogenic signals regulate miR-135b in gastric epithelial cells.* (A) Treatment of cytokines including IL-1α, IL-1β, TNF-α, lipopolysaccharide (LPS) or peptidoglycan from *Staphylococcus aureus* (PGN-sa) in wild-type gastric organoids and qRT-PCR measurement of miR-135b expression. (B, C) Comparing the effects of IL-1β and TNF-α on miR-135b expression in wild-type mouse gastric organoids over time (B), and in GIF-14 immortalized mouse gastric epithelial cells (C). (D, E) The inhibitory effects of the indicated MEK inhibitors on miR-135b expression as measured by qRT-PCR in GIF-14 (K-Ras^{G12V}) (D); and SNU-601 gastric carcinoma cells (E).

Figure 4. *Investigating the in vivo role of miR-135b in inflammation-induced gastric carcinogenesis.* (A) IL-1β mRNA levels in whole tissue samples from the stomachs of WT, K19-C2mE and Gan mice. (B) Correlation of miR-135b and IL-1β expression levels in WT, K19-C2mE and Gan whole tissue samples. (C) IL-1β mRNA levels in LMD-enriched WT epithelial cells, Gan carcinoma cells and Gan stromal cells. (D) Expression levels of miR-135b in WT, Gan and *Myd88(-/-)/*Gan. (E) Macroscopic photographs of miR-135b-proficient (*miR-135b-ln*$^{wt/wt}$; left) and miR-135b-deficient (*miR-135b-ln*$^{fl/fl}$; right) K19-C2mE mouse stomachs. (F) Representative H&E staining (top) and Ki-67 immunostaining (bottom) of

miR-135b-proficient (left) and miR-135b-deficient (right) K19-C2mE mouse stomach sections. Asterisks indicate Ki-67 positive proliferating zones. Scale bars, 200 μm (top) and 100 μm (bottom) (G, H) Scoring of hyperplastic gastric lesions (G) and Ki-67 positive cells (H) in miR-135b-proficient and miR-135b-deficient K19-C2mE mice. (I) Representative H&E staining (left), Ki-67 immunostaining (middle) and BaseScope *in situ* hybridization for miR-135b (right) in uninfected control (top) and *H. felis*-infected (bottom) wild-type mouse stomach 8 weeks post-infection (Scale bars, 100μm). Enlarged images of boxed areas of miR-135b BaseScope ISH are shown (Scale bars, 50μm). Arrows indicate infiltrated inflammatory cells in submucosa (left), and arrowheads indicate positive miR-135b detection as condensed dots (right). (J) The mean numbers of Ki-67 positive cells per gland (top) and miR-135b ISH dot (bottom) per gland in the uninfected control and *H. felis*-infected mouse stomach are shown (mean ± *s.d.*). Asterisk, $p < 0.05$.

Figure 5. *The in vitro tumorigenic activities of miR-135b in gastric epithelial cells*. (A) Soft agar colony formation assays were performed on AGS, SNU-638 and SNU-719 cells transfected with negative control mimic (Control) or miR-135b mimic (miR-135b). Left panels show cell colonies grown in soft agar, and graph on the right shows colony numbers relative to Control. (B) Ectopic expression of miR-135b increased migrated cell numbers SNU-638 and GIF-14 cells with in low basal miR-135b expression. In contrast, cell migration was abrogated by miR-135b inhibitor (TuD135) in SNU-601 cells with high basal miR-135b expression. (C) Sphere-forming assay after the transfection of negative control mimic (Control) or miR-135b mimic (miR-135b) into GIF-14 cell line.

Figure 6. *FOXN3 and RECK are direct target genes of miR-135b in gastric epithelial cells.* (A) A Venn diagram depicting the overlap of target genes predicted by computer algorithms

(TargetScan 7.1, StarBase 2.0 and microRNA.org) (red); genes downregulated in mouse gastritis lesion or tumors (blue); and gene downregulated in our human gastric tumors in the TCGA data set for stomach adenocarcinoma (green). Putative target genes identified by this approach are listed, which includes *FOXN3* and *RECK*. (B) The construction of luciferase reporter vectors with inserted wild type or mutant *FOXN3* and *RECK* 3'-UTR sequences. (C, D) Changes in the normalized reporter gene activities of wild-type and mutant *FOXN3* (C) and *RECK* (D) 3'-UTR luciferase reporter constructs in response to the co-transfection of negative control (NC) or miR-135b mimic in SNU-638 cells. (E) The effects of miR-135b mimic, siRNA again *FOXN3* or *RECK* and negative control mimic (NC) on the migration of transfected SNU-638 cells in Transwell migration assays. (top) Fluorescent staining of migrated cells; (bottom) graphical presentation of migrated cell numbers. (F, G) The relative *Foxn3* and *Reck* expression levels (left) and their correlation with miR-135b levels (right) in WT, K19-C2mE and Gan samples. (G) The relative expression levels of *FOXN3* and *RECK* in normal gastric tissues (N) and gastric tumors (T) (left) and their correlation with miR-135b expression in the TCGA data set for stomach adenocarcinoma (STAD).

Figure 1.

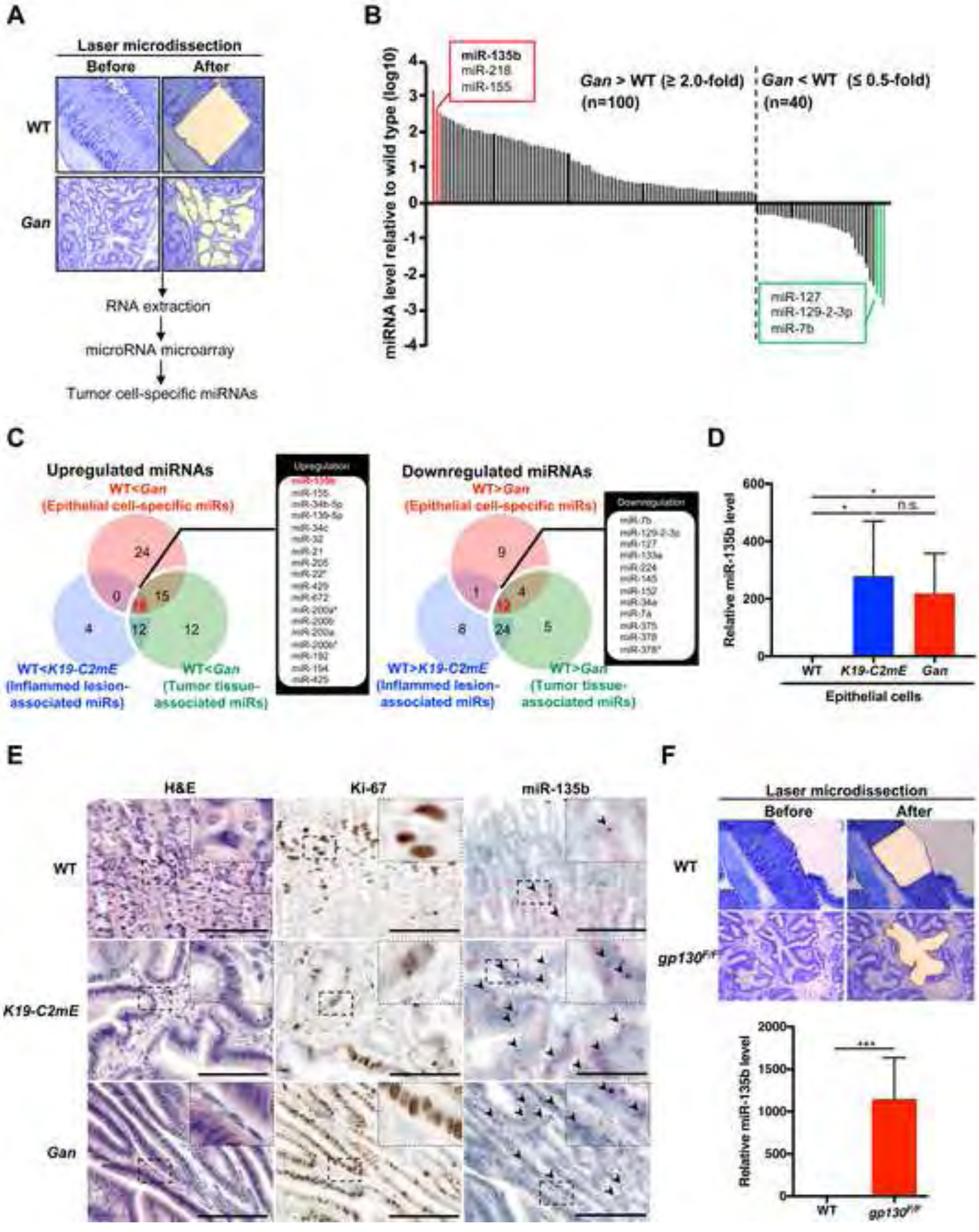
A
Laser microdissection
Before
After
WT
Gan
RNA extraction
microRNA microarray
Tumor cell-specific miRNAs
B
miR-135b
miR-218
miR-155
Gan > WT (≥ 2.0-fold)
(n=100)
Gan < WT (≤ 0.5-fold)
(n=40)
miR-127
miR-129-2-3p
miR-7b
miRNA level relative to wild type (log10)
C
Upregulated miRNAs
WT<Gan
(Epithelial cell-specific miRs)
WT<K19-C2mE
(Inflammed lesion-associated miRs)
WT<Gan
(Tumor tissue-associated miRs)
Downregulated miRNAs
WT>Gan
(Epithelial cell-specific miRs)
WT>K19-C2mE
(Inflammed lesion-associated miRs)
WT>Gan
(Tumor tissue-associated miRs)
D
Relative miR-135b level
WT
K19-C2mE
Gan
Epithelial cells
n.s.
E
H&E
Ki-67
miR-135b
WT
K19-C2mE
Gan
F
Laser microdissection
Before
After
WT
gp130F/F
Relative miR-135b level
WT
gp130F/F

Figure 2.

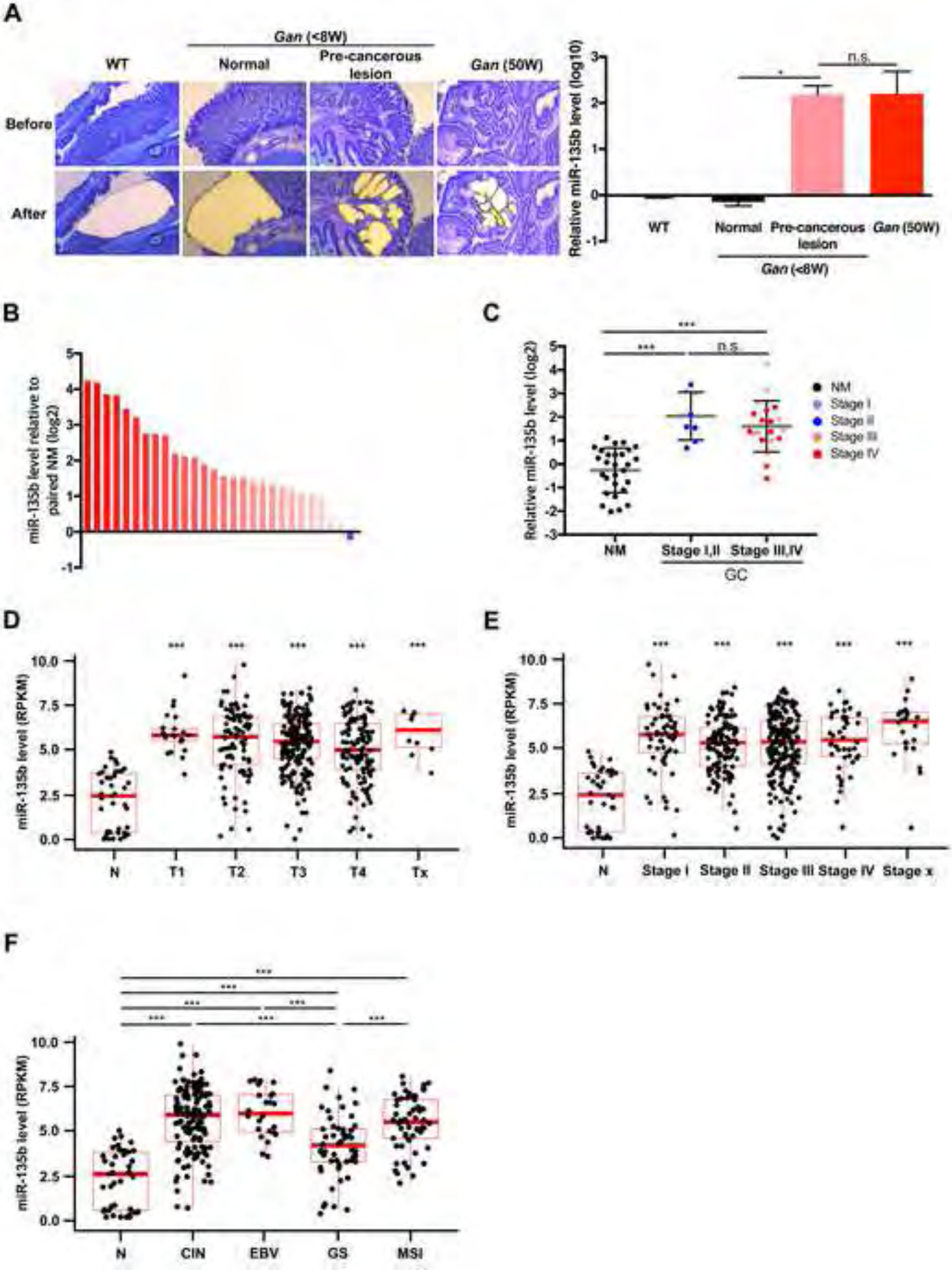
A
Gan (<8W)
WT
Normal
Pre-cancerous lesion
Gan (50W)
Before
After
Relative miR-135b level (log10)
n.s.
*
WT
Normal
Pre-cancerous lesion
Gan (50W)
Gan (<8W)
B
miR-135b level relative to paired NM (log2)
C
Relative miR-135b level (log2)
***
n.s.
NM
Stage I
Stage II
Stage III
Stage IV
NM
Stage I,II
Stage III,IV
GC
D
miR-135b level (RPKM)
N
T1
T2
T3
T4
Tx
E
miR-135b level (RPKM)
N
Stage I
Stage II
Stage III
Stage IV
Stage x
F
miR-135b level (RPKM)
N
CIN
EBV
GS
MSI

Figure 3.

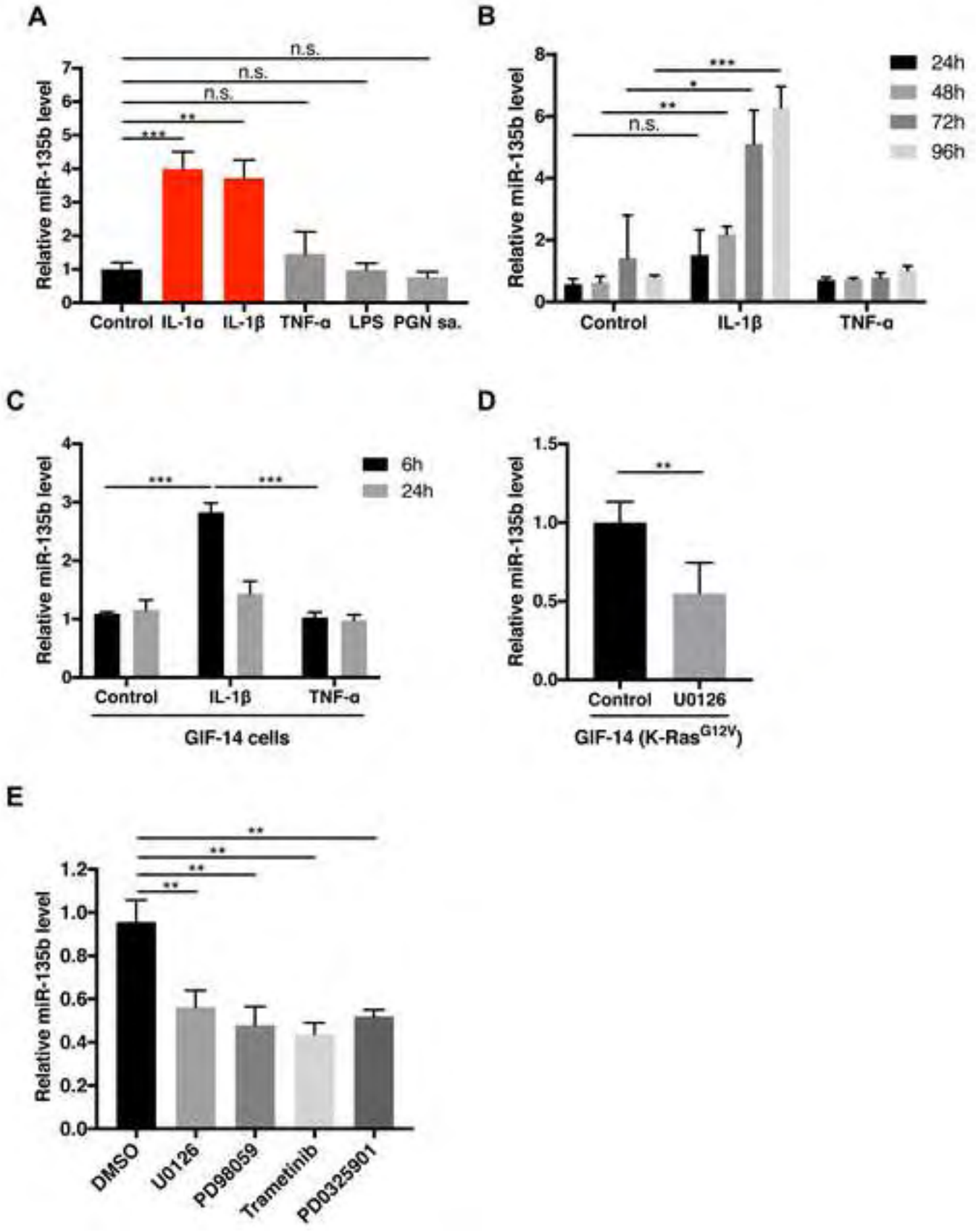
A
Relative miR-135b level
n.s.
n.s.
n.s.
**
***
Control
IL-1α
IL-1β
TNF-α
LPS
PGN sa.
B
Relative miR-135b level
***
*
**
n.s.
24h
48h
72h
96h
Control
IL-1β
TNF-α
C
Relative miR-135b level
***
***
6h
24h
Control
IL-1β
TNF-α
GIF-14 cells
D
Relative miR-135b level
**
Control
U0126
GIF-14 (K-Ras^{G12V})
E
Relative miR-135b level
**
**
**
**
DMSO
U0126
PD98059
Trametinib
PD0325901

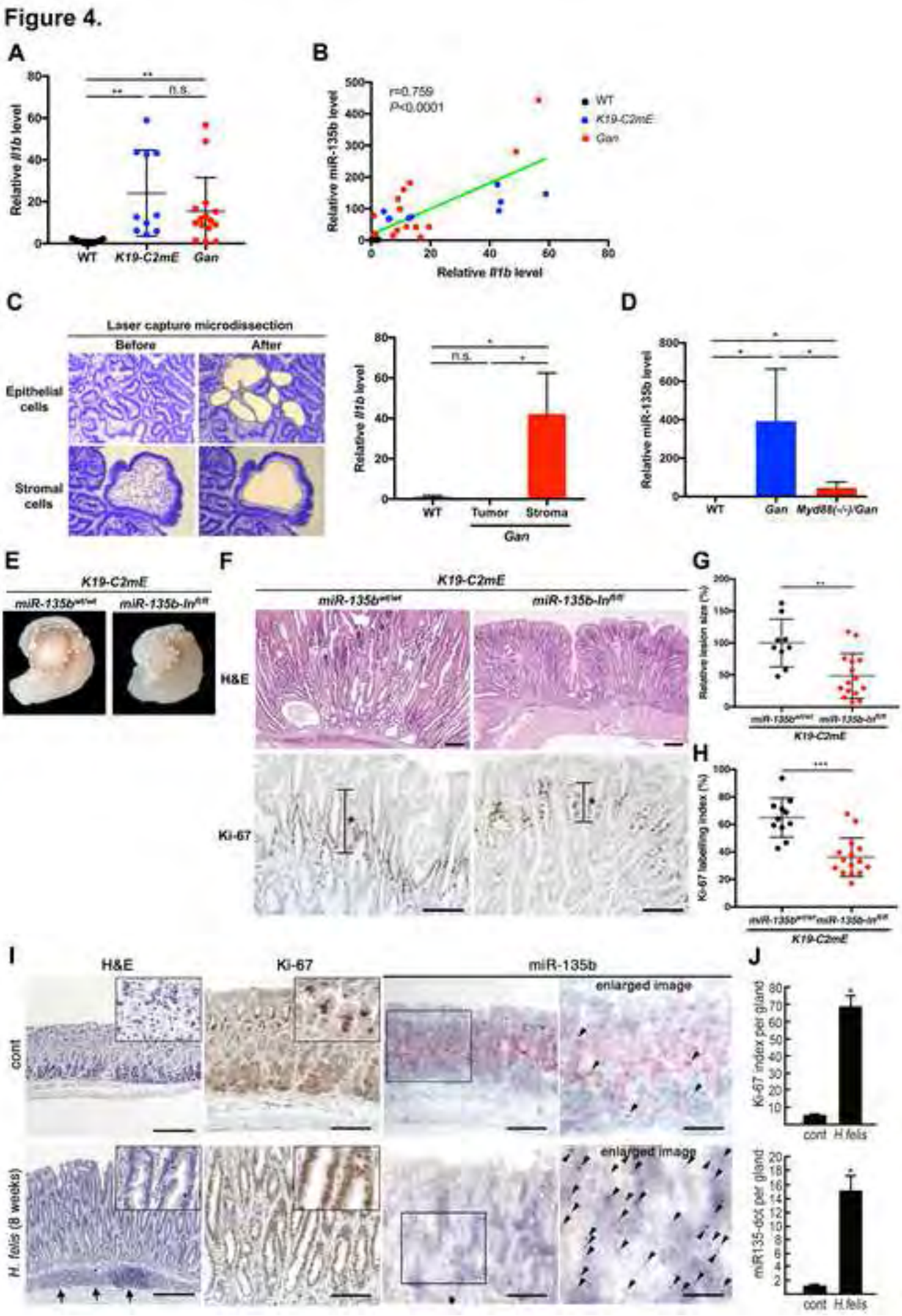
Figure 4.
A
Relative Il1b level
WT
K19-C2mE
Gan
n.s.
B
r=0.759
P<0.0001
WT
K19-C2mE
Gan
Relative miR-135b level
Relative Il1b level
C
Laser capture microdissection
Before
After
Epithelial cells
Stromal cells
Relative Il1b level
n.s.
WT
Tumor
Stroma
Gan
D
Relative miR-135b level
WT
Gan
Myd88(-/-)/Gan
E
K19-C2mE
miR-135b^wt/wt
miR-135b-In^f/f
F
K19-C2mE
miR-135b^wt/wt
miR-135b-In^f/f
H&E
Ki-67
G
Relative lesion size (%)
miR-135b^wt/wt
miR-135b-In^f/f
K19-C2mE
H
Ki-67 labeling index (%)
miR-135b^wt/wtmiR-135b-In^f/f
K19-C2mE
I
H&E
Ki-67
miR-135b
enlarged image
cont
H. felis (8 weeks)
J
Ki-67 index per gland
cont
H.felis
miR135-dot per gland
cont
H.felis

Figure 5.

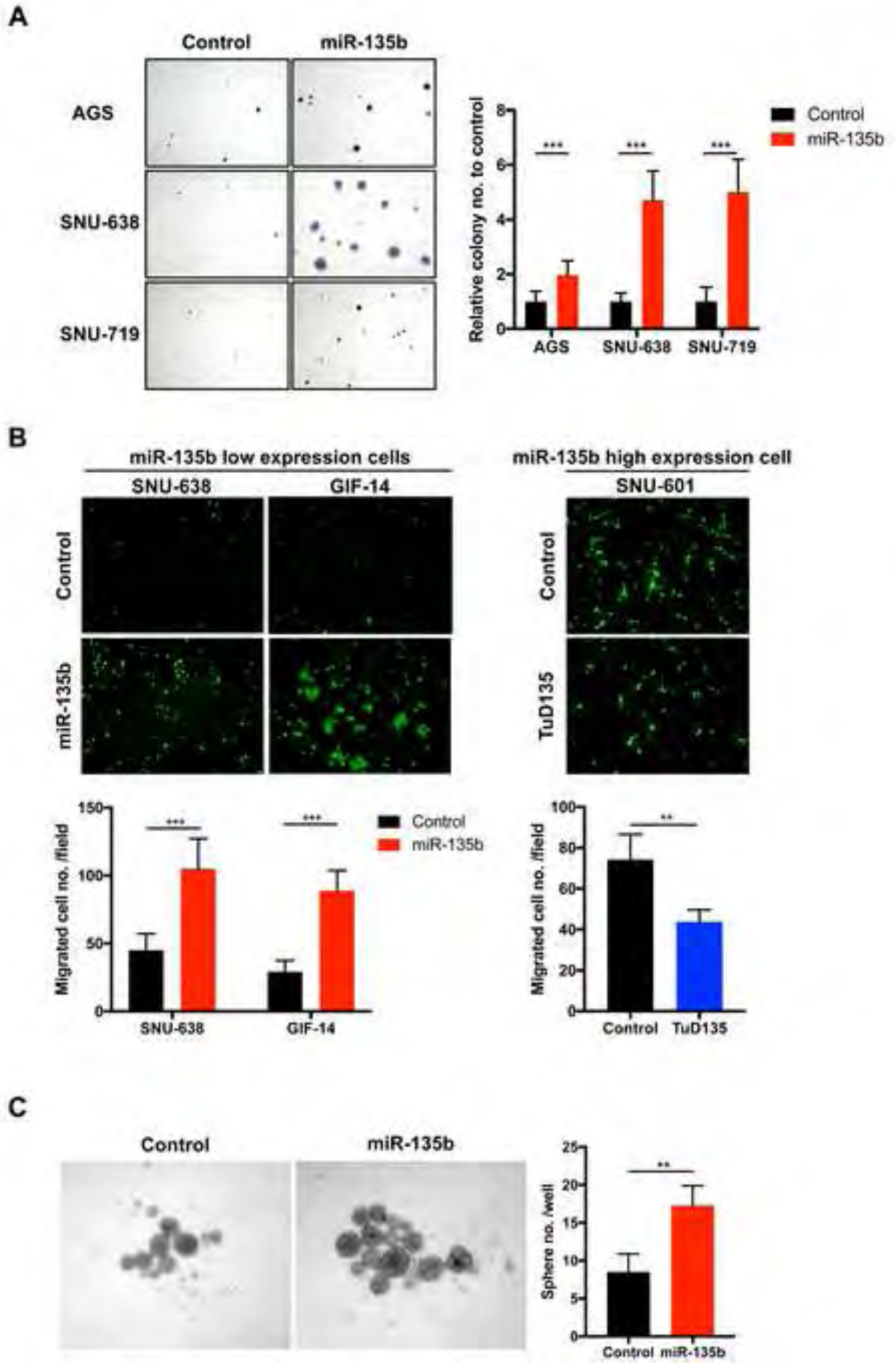
A
Control
miR-135b
AGS
SNU-638
SNU-719
Relative colony no. to control
Control
miR-135b
***
AGS
SNU-638
SNU-719
B
miR-135b low expression cells
miR-135b high expression cell
SNU-638
GIF-14
SNU-601
Control
miR-135b
TuD135
Migrated cell no. /field
**
C
Control
miR-135b
Sphere no. /well

Figure 6.

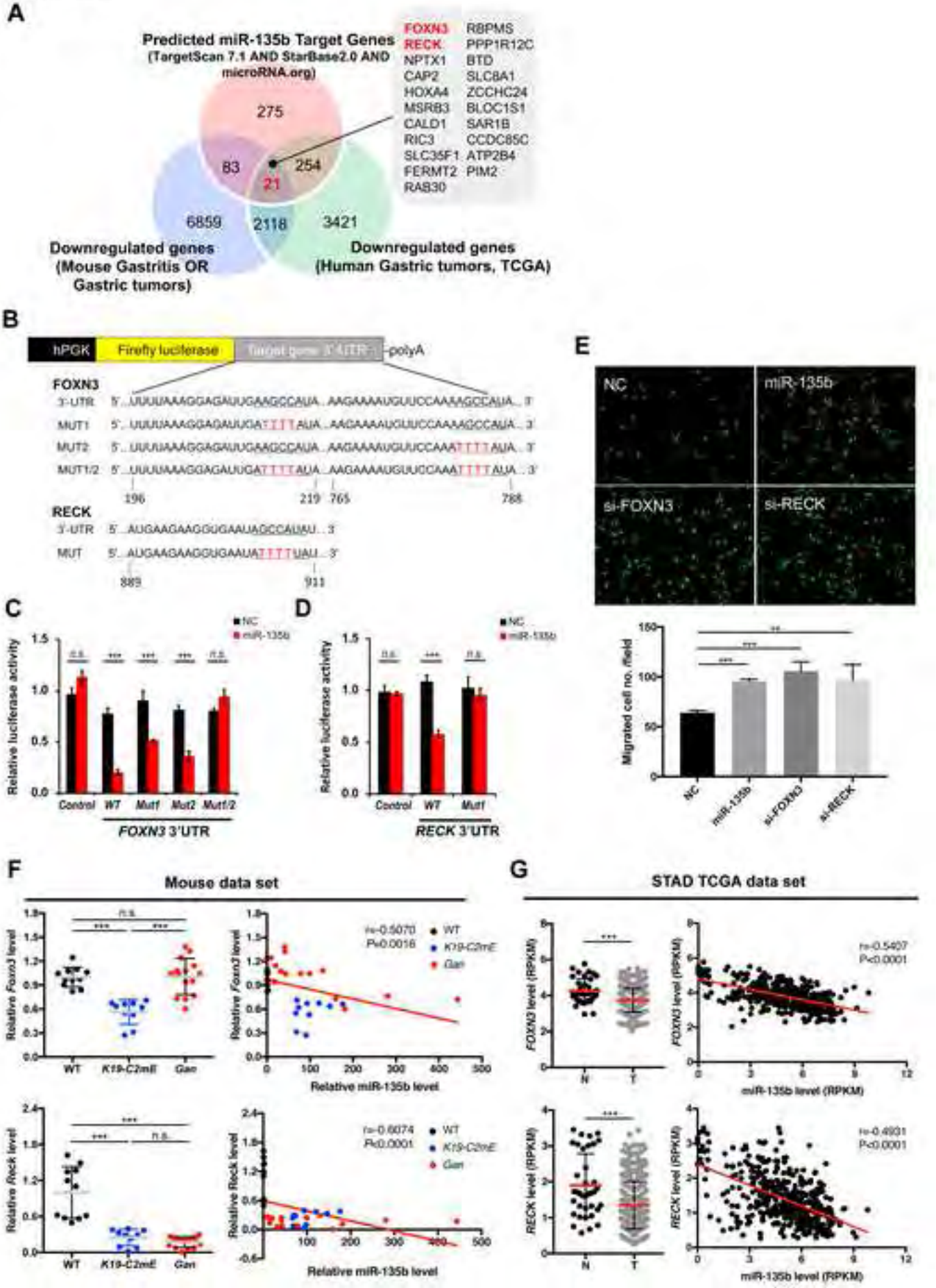
A
Predicted miR-135b Target Genes
(TargetScan 7.1 AND StarBase2.0 AND microRNA.org)
275
83
254
21
6859
2118
3421
Downregulated genes (Mouse Gastritis OR Gastric tumors)
Downregulated genes (Human Gastric tumors, TCGA)
FOXN3 RBPMS
RECK PPP1R12C
NPTX1 BTD
CAP2 SLC8A1
HOXA4 ZCCHC24
MSRB3 BLOC1S1
CALD1 SAR1B
RIC3 CCDC85C
SLC35F1 ATP2B4
FERMT2 PIM2
RAB30
B
hPGK
Firefly luciferase
polyA
FOXN3
3'-UTR
MUT1
MUT2
MUT1/2
RECK
MUT
C
Relative luciferase activity
NC
miR-135b
Control
WT
Mut1
Mut2
Mut1/2
FOXN3 3'UTR
D
RECK 3'UTR
E
NC
miR-135b
si-FOXN3
si-RECK
Migrated cell no. /field
F
Mouse data set
Relative Foxn3 level
Relative miR-135b level
WT
K19-C2mE
Gan
Relative Rock level
G
STAD TCGA data set
FOXN3 level (RPKM)
miR-135b level (RPKM)
RECK level (RPKM)

"WHAT YOU NEED TO KNOW"

BACKGROUND AND CONTEXT: *Helicobacter pylori*-induced gastritis is strongly associated with human gastric cancer. However, epithelial cell-specific changes in microRNA expression during this remains poorly characterized due to tissue heterogeneity. [26 words]

NEW FINDINGS: miR-135b is strongly induced in epithelial cells during *H. felis* - or COX2/IL-1-induced gastritis and early gastric carcinogenesis. It mediates its function by suppressing *FOXN3* and *RECK*. [27 words]

LIMITATIONS: Although miR-135b is functionally important in mediating gastritis *in vivo* and promotes tumorigenicity *in vitro*, its contribution to cancer progression and metastasis remains to be clarified. [26 words]

IMPACT: miR-135b is a key regulatory node connecting physiologic inflammation and tissue repair. Its aberrant expression promotes a hyperplastic pre-neoplastic state, which can be of diagnostic and therapeutic application. [28 words]

"LAY SUMMARY"

MicroRNA-135b is strongly induced in gastritis and early gastric carcinogenesis. It functionally links inflammation and pre-neoplastic hyperplasia. This insight could help with the early intervention and diagnosis of gastric cancer. [30 words]

Figure S1

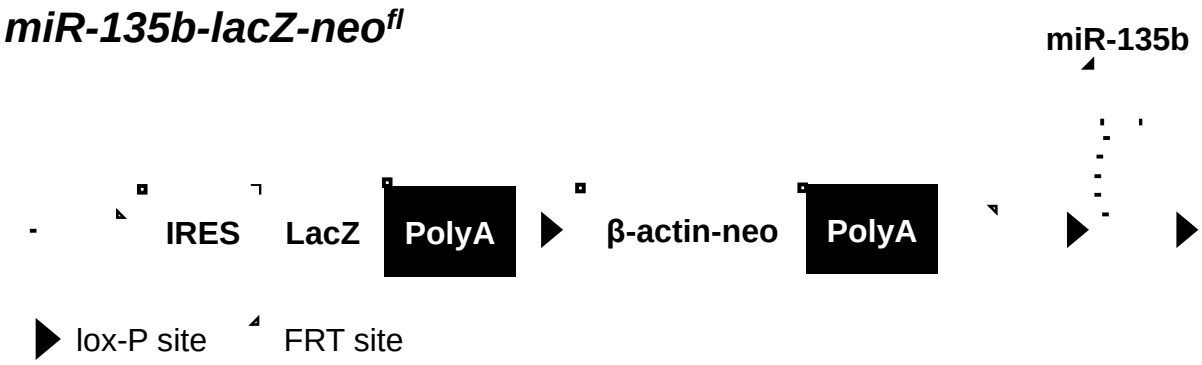

Figure S2

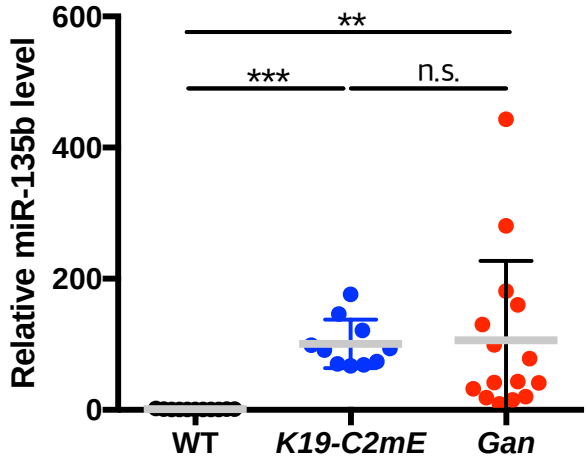

Figure S3

A


0 ng/ml
0.5 ng/ml
2.5 ng/ml
50 ng/ml

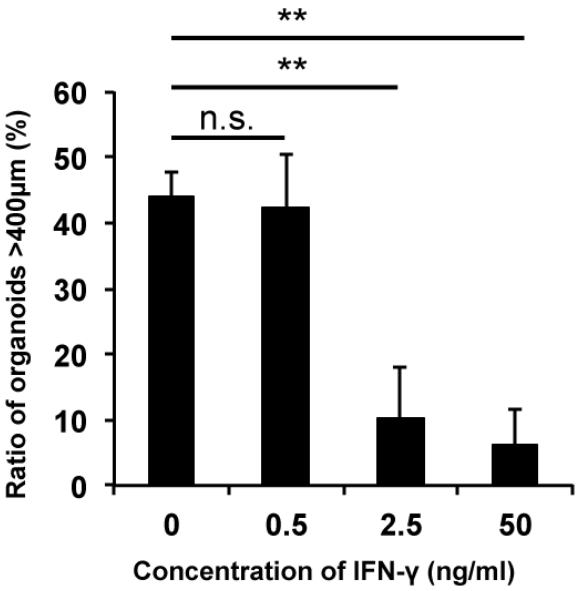
**
**
n.s.
Ratio of organoids >400μm (%)
60
50
40
30
20
10
0
0
0.5
2.5
50
Concentration of IFN-γ (ng/ml)

B

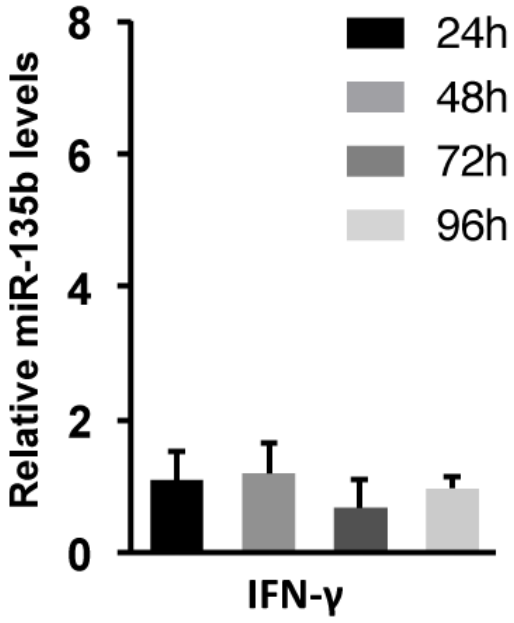
Relative miR-135b levels
8
6
4
2
0
24h
48h
72h
96h
IFN-γ

Figure S4

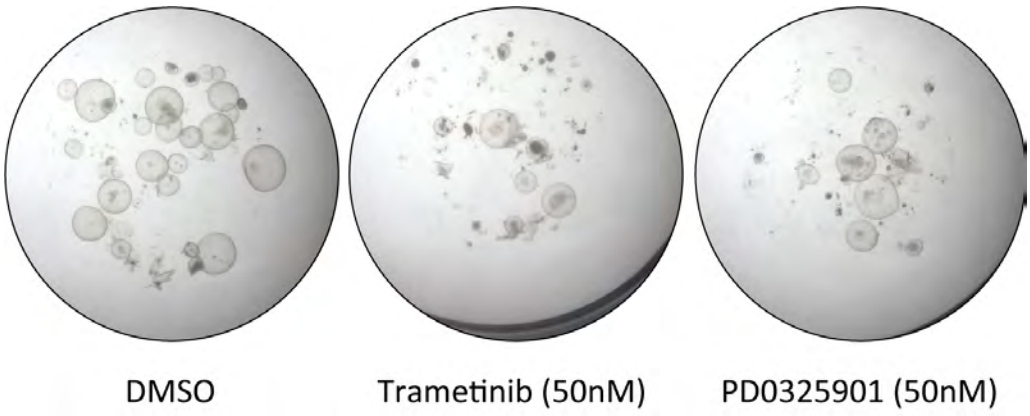
DMSO
Trametinib (50nM)
PD0325901 (50nM)

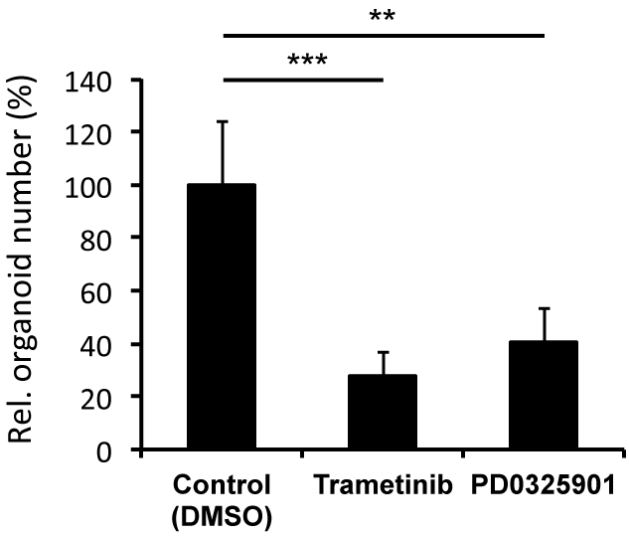
**
***
Rel. organoid number (%)
140
120
100
80
60
40
20
0
Control (DMSO)
Trametinib
PD0325901

Figure S5

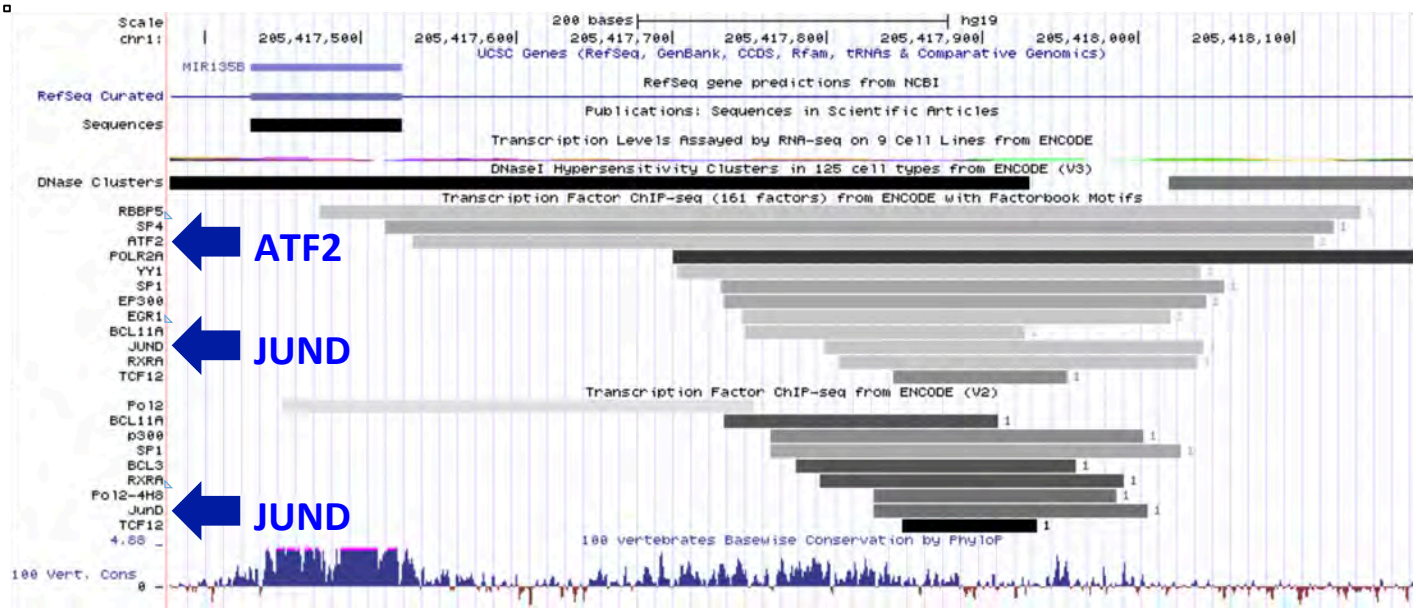
Scale
chr1:
200 bases
hg19
205,417,500
205,417,600
205,417,700
205,417,800
205,417,900
205,418,000
205,418,100
UCSC Genes (RefSeq, GenBank, CCDS, Rfam, tRNAs & Comparative Genomics)
MIR135B
RefSeq Curated
RefSeq gene predictions from NCBI
Sequences
Publications: Sequences in Scientific Articles
Transcription Levels Assayed by RNA-seq on 9 Cell Lines from ENCODE
DNase Clusters
DNaseI Hypersensitivity Clusters in 125 cell types from ENCODE (V3)
Transcription Factor ChIP-seq (161 factors) from ENCODE with Factorbook Motifs
RBBP5
SP4
ATF2
POLR2A
YY1
SP1
EP300
EGR1
BCL11A
JUND
RXRA
TCF12
ATF2
JUND
Transcription Factor ChIP-seq from ENCODE (V2)
Pol2
BCL11A
p300
SP1
BCL3
RXRA
Pol2-4H8
JunD
TCF12
JUND
4.88
100 vertebrates Basewise Conservation by PhyloP
100 Vert. Cons
0

Figure S6

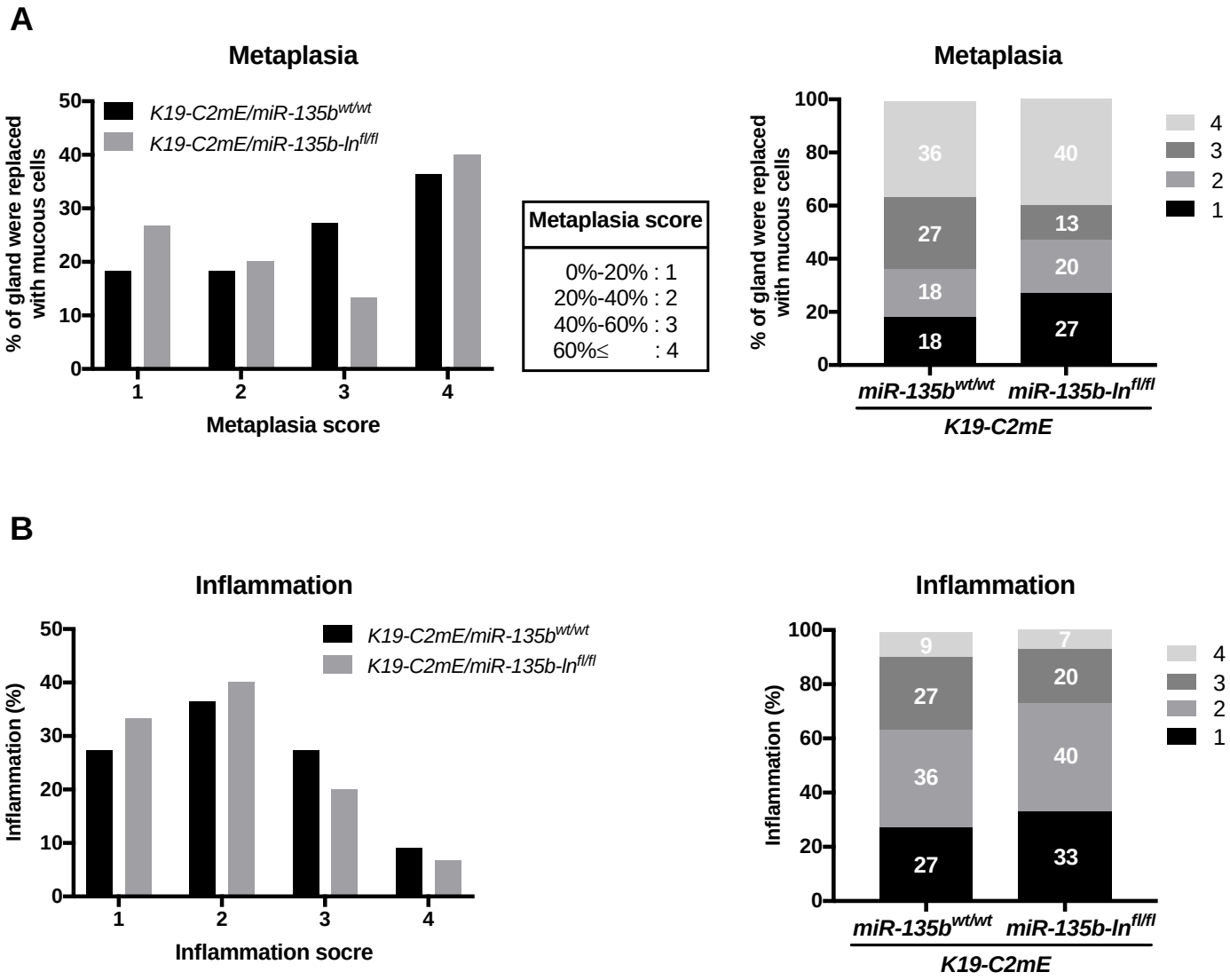
A
Metaplasia
% of gland were replaced with mucous cells
K19-C2mE/miR-135b^wt/wt
K19-C2mE/miR-135b-ln^fl/fl
Metaplasia score
Metaplasia score
0%-20% : 1
20%-40% : 2
40%-60% : 3
60%≤ : 4
Metaplasia
% of gland were replaced with mucous cells
36
27
18
18
40
13
20
27
4
3
2
1
miR-135b^wt/wt
miR-135b-ln^fl/fl
K19-C2mE
B
Inflammation
Inflammation (%)
K19-C2mE/miR-135b^wt/wt
K19-C2mE/miR-135b-ln^fl/fl
Inflammation socre
Inflammation
Inflammation (%)
9
27
36
27
7
20
40
33
4
3
2
1
miR-135b^wt/wt
miR-135b-ln^fl/fl
K19-C2mE

Figure S7

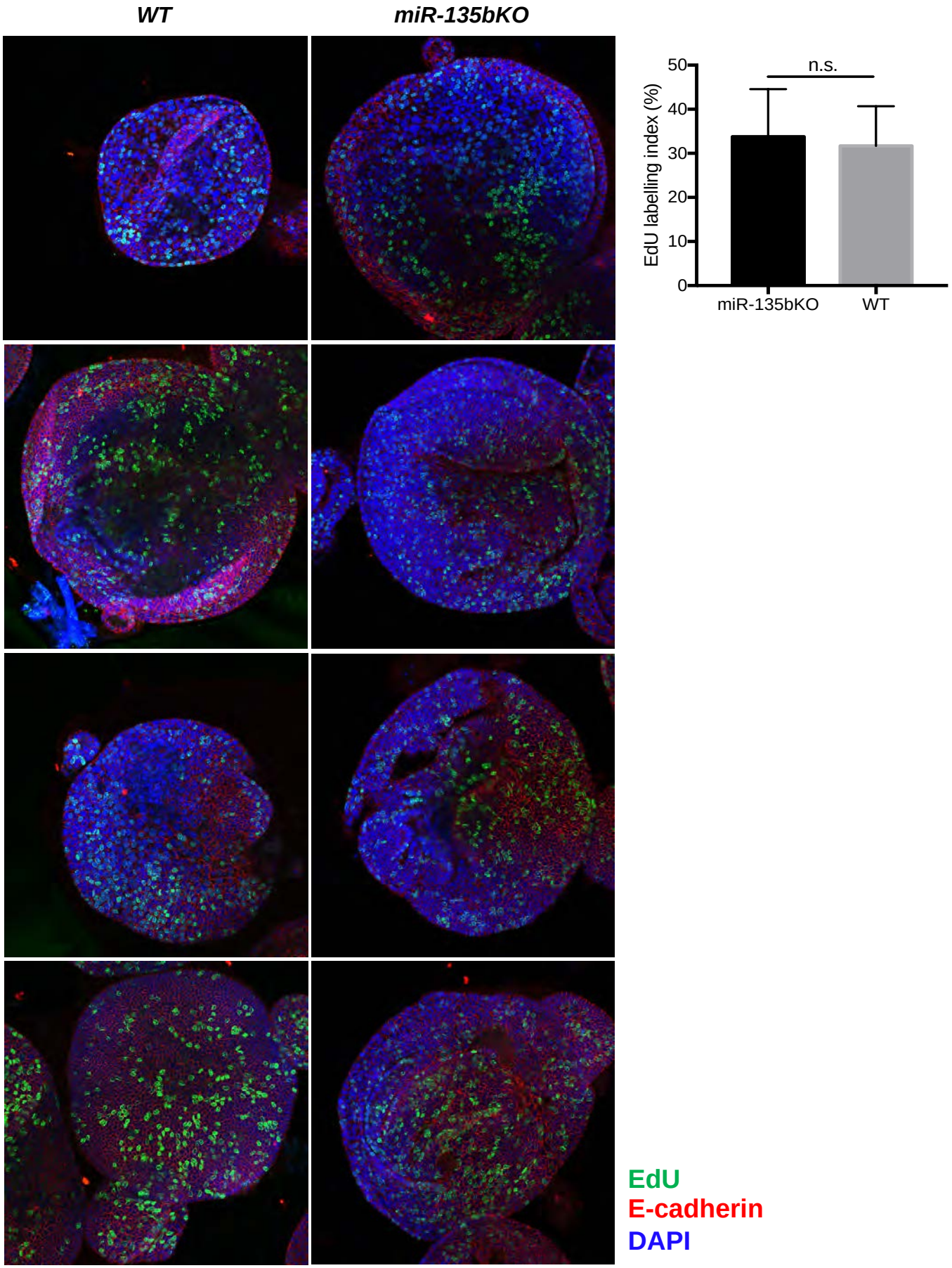
WT
miR-135bKO
n.s.
EdU labelling index (%)
50
40
30
20
10
0
miR-135bKO
WT
EdU
E-cadherin
DAPI

Figure S8

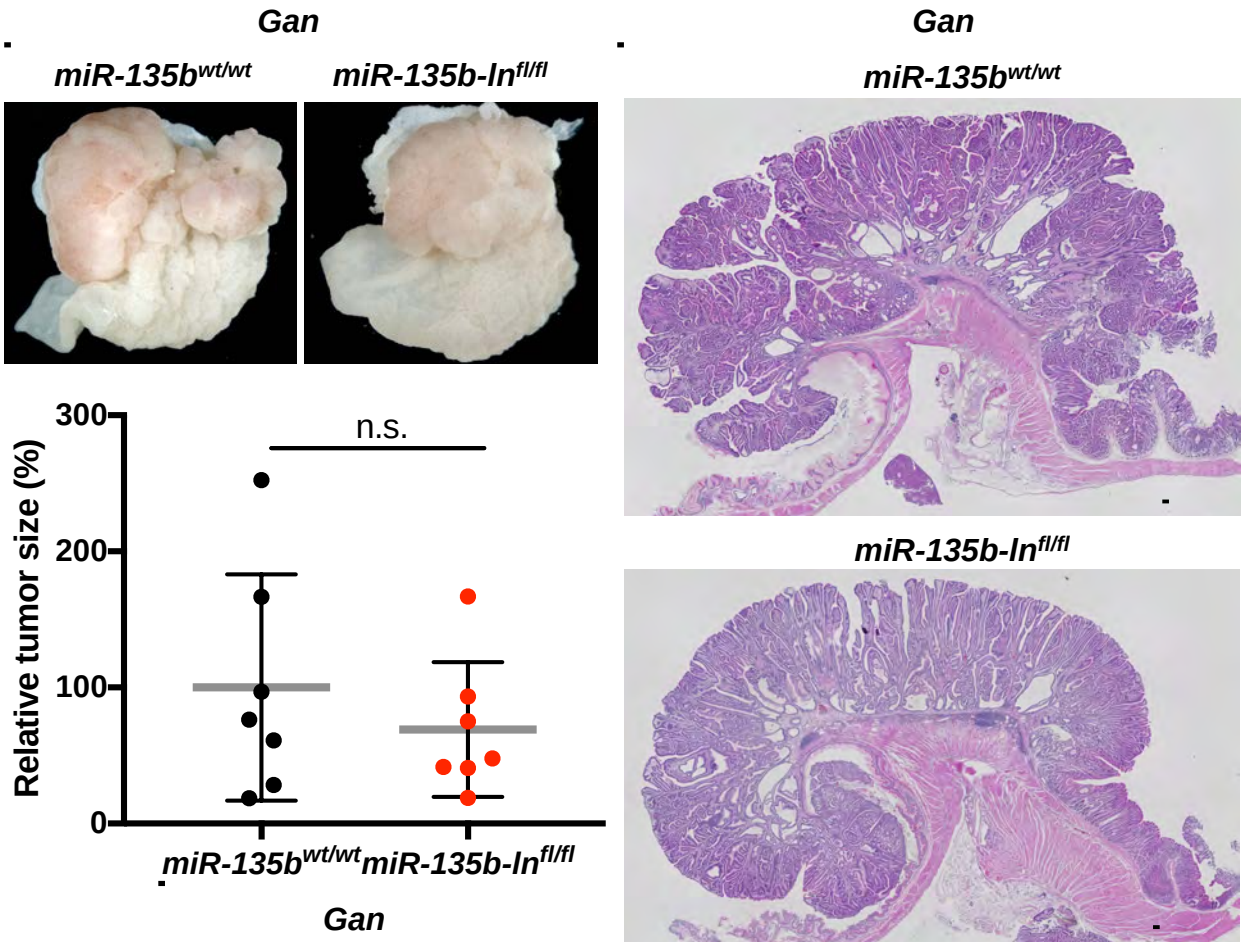
Gan
miR-135b^wt/wt
miR-135b-ln^fl/fl
300
200
100
0
Relative tumor size (%)
n.s.
miR-135b^wt/wt
miR-135b-ln^fl/fl
Gan
Gan
miR-135b^wt/wt
miR-135b-ln^fl/fl

Figure S9

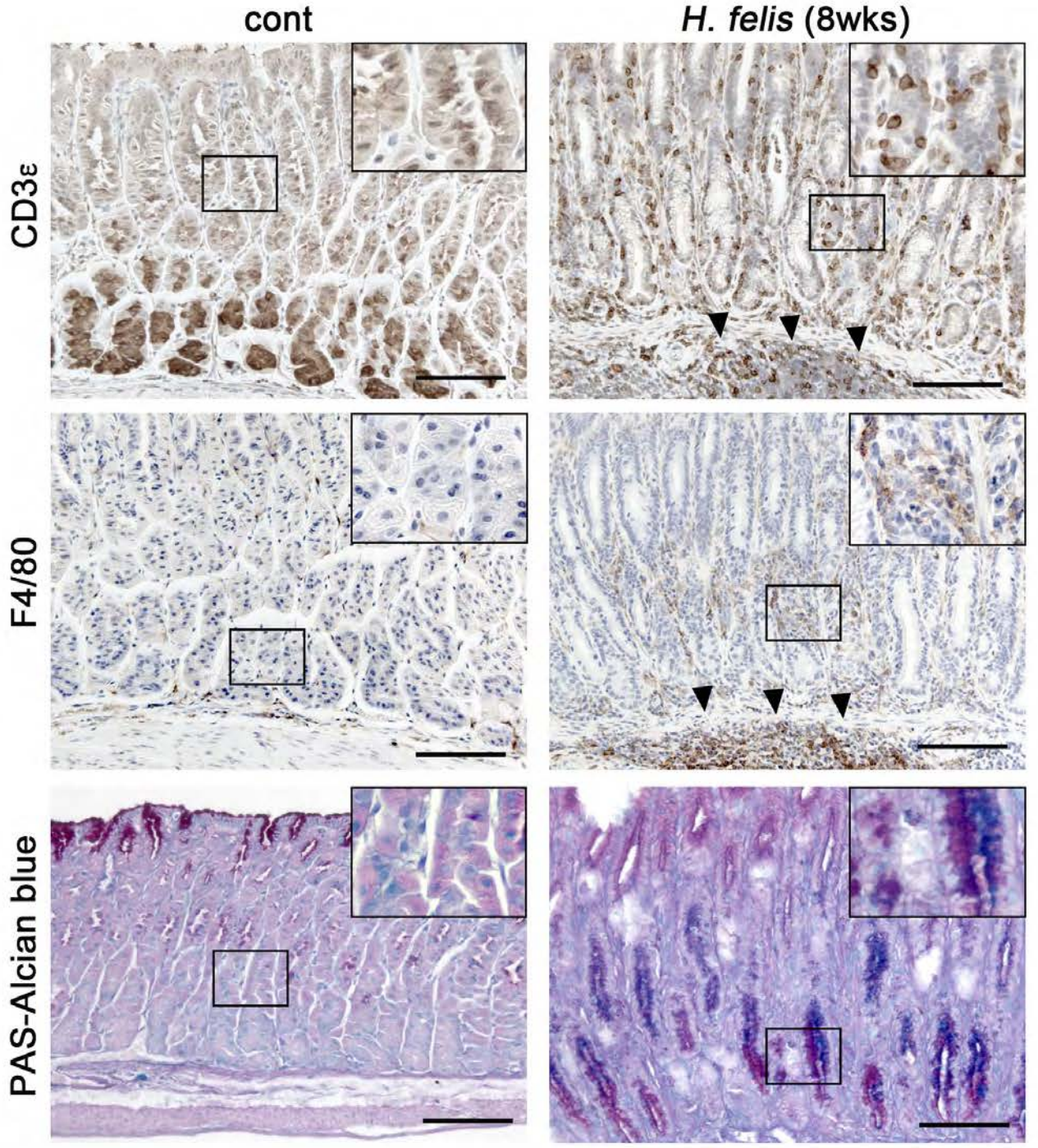

Figure S10

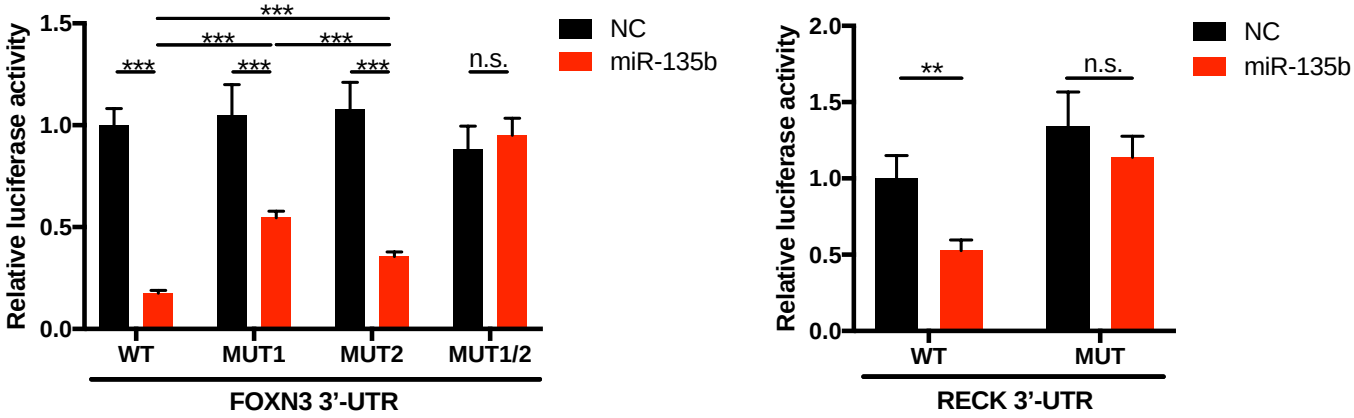
Relative luciferase activity
1.5
1.0
0.5
0.0
***
***
***
***
***
n.s.
NC
miR-135b
WT
MUT1
MUT2
MUT1/2
FOXN3 3'-UTR
Relative luciferase activity
2.0
1.5
1.0
0.5
0.0
**
n.s.
NC
miR-135b
WT
MUT
RECK 3'-UTR

Figure S11

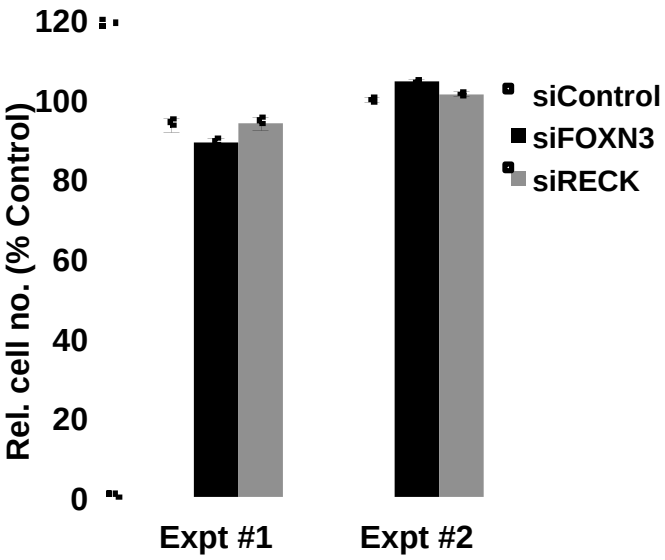
120
100
80
60
40
20
0
Rel. cell no. (% Control)
Expt #1
Expt #2
siControl
siFOXN3
siRECK

Figure S12

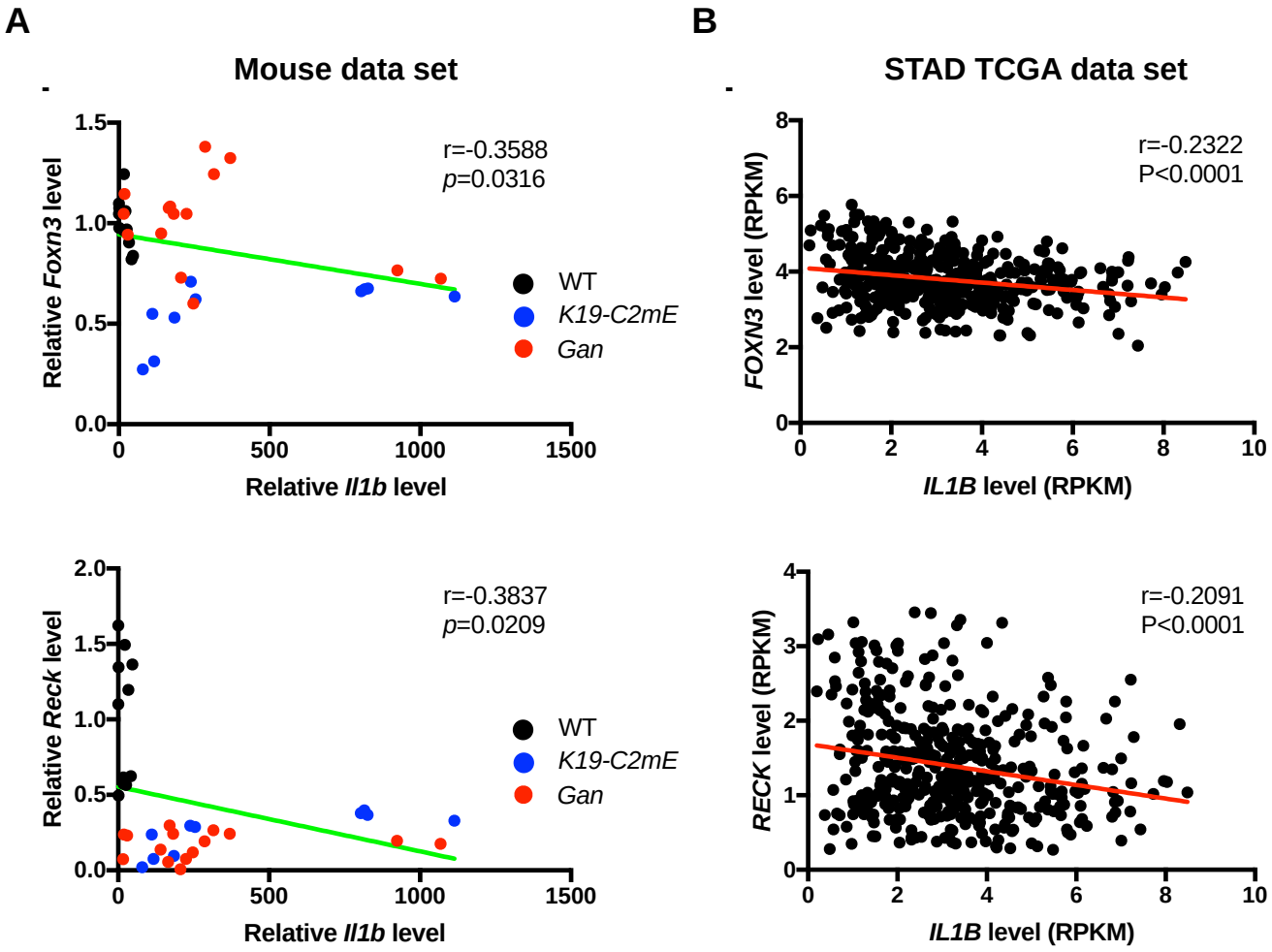
A
Mouse data set
r=-0.3588
p=0.0316
WT
K19-C2mE
Gan
Relative Foxn3 level
Relative Il1b level
r=-0.3837
p=0.0209
Relative Reck level
B
STAD TCGA data set
r=-0.2322
P<0.0001
FOXN3 level (RPKM)
IL1B level (RPKM)
r=-0.2091
P<0.0001
RECK level (RPKM)

Figure S13

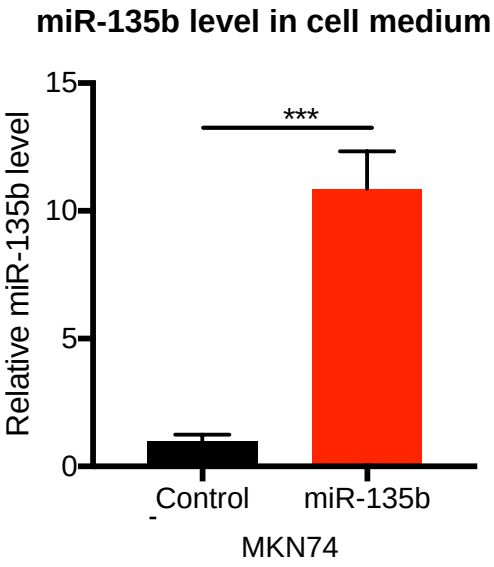
miR-135b level in cell medium
Relative miR-135b level
15
10
5
0
***
Control
miR-135b
MKN74

Supplementary Material

SUPPLEMENTARY METHODS AND MATERIALS

Histology and scoring of proliferation, metaplasia and inflammation

The sizes of hyperplastic and cancerous lesions were measured by the ImageJ 1.46 software program (NIH, Bethesda, MD, USA)[1] using photographs that were taken under a dissecting microscope. The mucosal thickness (height) of hyperplastic lesions was measured using histology sections. The 'lesion size' was calculated by multiplying the area by the height, as previously described[2]. The relative lesion size was calculated in comparison with the mean of miR-135b-proficient (*miR-135b*$^{wt/wt}$) K19-C2mE lesion size as 100%.

Mouse stomach tissues were fixed in 4% paraformaldehyde, paraffin-embedded, and sectioned at 4-μm thickness. The sections were stained with H&E or immunohistochemistry using antibodies against Ki67 antibody (Life Technologies, Grand Island, NY, USA), CD3ε (Santa Cruz Biotechnology, Dallas, TX, USA) and F4/80 (Bio-Rad, Hercules, CA, USA). For Ki67 labeling index, the mean number of Ki67-positive cells per gland (5 glands for each mouse) were calculated. For metaplasia scoring, the replacement areas of mucosa with mucous cells were measured using H&E sections, and graded 1 to 4 according to the replacement area with 0-20%, 20-40%, 40-60%, and >60%, respectively. Inflammation scoring from grade 1 to 4 was performed as detailed in a published protocol[3].

Organoid Culture

Gastric organoids were cultured as described by Barker *et al.*[4], in growth factor reduced Matrigel (Corning) with Advanced DMEM/F12 medium (Invitrogen) supplemented with 10% FBS and penicillin and streptomycin, and with 10% R-spondin conditional medium,

GlutaMax (Invitrogen), 10mM HEPES (Sigma), N2 supplement (Invitrogen), B27 supplement (Invitrogen), 1 μM N-Acetylcystein (Sigma), 50 ng/ml mouse EGF (Invitrogen), 100 ng/ml human recombinant FGF10 (PeproTech), 10 nM Gastrin (Sigma-Aldrich), 10 μM Y-27632 (Wako), 5 μM CHIR99021 (Tocris Bioscience), 100 ng/ml Noggin (Peprotech). After 3 days, 100 ng/ml of IL-1α (Wako), 100 ng/ml IL-1β (Wako), 100 ng/ml tumor necrosis factor-α (TNF-α; Wako), the indicated concentrations of interferon-γ (IFN-γ; PeproTech), lipopolysaccharide (LPS; Wako) or peptidoglycan from Staphylococcus aureus (PGN-SA; InvivoGen, San Diego, CA, USA) were added into the gastric organoids cultures for the indicated duration.

EdU labelling of cultured gastric organoids

Cellular proliferation within gastric organoids was assessed using the Click-it EdU Imaging kit (Invitrogen) following the supplied protocol. Organoids were labelled with EdU for 10 min, which was then followed by immunofluorescent staining with anti-E-cadherin antibody (R&D) and Alexa Fluor 488 secondary antibody (Molecular Probes). The stained organoids were analyzed using a Leica TCS SP8 laser-scanning microscope (Leica).

Luciferase reporter assays

The pmirGLO Dual Luciferase reporter vector ((Promega) containing the 3'-UTR of *FOXN3* or *RECK* were transiently transfected into HEK293 cells (ATCC) cultured in standard growth conditions, together with control or miR-135b mimic microRNAs. Cells were harvested 24h post transfection and assayed for firefly luciferase and *Renilla* luciferase activities on a Centro XS^3 LB960 luminometer (Berthold Technologies).

SUPPLEMENTARY FIGURE LEGENDS

Figure S1. *Generation of miR-135b-deficient mice.* A schematic illustrating the interruption of miR-135b transcription in the *miR-135b-lacZ-neo*^{fl} (abbreviated as *miR-135b-ln*^{fl}) allele by the insertion of polyA signals upstream of miR-135b. This allele is then introduced into the *K19-C2mE* gastritis or *Gan* gastric cancer mouse models.

Figure S2. *miR-135b levels in whole tissue samples for WT, K19-C2mE and Gan.* Analysis of miR-135b expression by qRT-PCR in whole tissue samples prepared from wild-type (WT), *K19-C2mE* and *Gan* mouse stomachs. Expression of miR-135b ± SD is expressed relative to WT levels. $^{**}P < 0.01$, $^{***}P < 0.001$, n.s., not significant.

Figure S3. *Determining the effects of IFN-γ on miR-135b expression in gastric organoids.* (A) The cytotoxic effects of IFN-γ. Representative images of wild-type gastric organoids cultured in the presence of increasing concentrations of IFN-γ (left); and their effects on the successful expansion of organoids (>400 μm), as a ratio of total organoid numbers (right). (B) The effects of IFN-γ (0.5ng/ml) on miR-135b expression levels in gastric organoids over time.

Figure S4. *MEK inhibitor suppresses gastric organoid growth.* Representative images showing the toxic effects of MEK inhibitors trametinib (50 nM) and PD0325901 (50nM) on the growth in wild-type gastric organoids compared with the DMSO treated control (top). Organoids generated from three separate wild type mice were treated and the resultant number of organoids were counted and expressed as a ratio to the corresponding DMSO-treated control for each mouse (bottom).

Figure S5. *Occupancies of ATF2 and JUND transcription factors on the proximal miR-135b promoter.* Excerpt from the USCS Genome Browser (GRCh37hg19; http://genome.ucsc.edu) showing the enrichment of genomic fragments within the proximal miR-135b promoter in the indicated ChIP-Seq experiments, performed by the ENCODE project[5, 6]. Blue arrows indicate the distribution of genomic fragments enriched by the ATF2 (Activating Transcription Factor 2) and JUND (JunD subunit of the heterodimeric AP-1 transcription factor).

Figure S6. *Measurement of mucous cell metaplasia and inflammation* (A) Mucous cell metaplasia in miR-135b-proficient and -deficient *K19-C2mE* mouse stomachs were scored by measuring the area of the mucosa replaced with mucous cells. (B) Scoring of inflammation in miR-135b-proficient and -deficient *K19-C2mE* mouse stomachs.

Figure S7. *The effects of miR-135b-deficiency on gastric organoids proliferation.* (Left) Confocal microscopy images of wild-type (*miR-135b-ln*$^{wt/wt}$*;* WT) and miR-135b-deficient (*miR-135b-ln*$^{fl/fl}$; miR-135bKO) organoids stained for EdU (green) and E-cadherin (red) and nuclear DNA with DAPI (blue). (Right) The EdU labelling index of 10 representative gastric organoids of each genotype is presented as mean ± SD; n.s., not significant.

Figure S8. *The effect of miR-135b-deficiency on gastric tumorigenicity of Gan mice.* (Top left) Macroscopic photographs of miR-135b-proficient (*miR-135b-ln*$^{wt/wt}$) and miR-135b-deficient (*miR-135b-ln*$^{fl/fl}$) *Gan* stomachs. (Bottom left) *miR-135b-ln*$^{wt/wt}$ and *miR-135b-ln*$^{fl/fl}$ *Gan* mouse stomach tumor sizes (mean ± SD; n.s., not significant). (Right) Representative

H&E staining for *miR-135b-ln*$^{wt/wt}$ (top) and *miR-135b-ln*$^{fl/fl}$ (bottom) *Gan* mouse stomach tissues. The scale bars indicate 1000 μm.

Figure S9. *H. felis infection induced profound gastric inflammation*. Representative photographs of immunostaining for CD3ε (top) and F4/80 (middle) and PAS-Alcian blue staining (bottom) in uninfected control wild-type mouse stomach (left) and those infected with *H. felis* for 8 weeks (right). Inserts are magnified images of indicated sections and arrowheads indicate infiltrated inflammatory cells in the sub-mucosa. Scale bars, 100μm.

Figure S10. *Luciferase assay of the targeting of FOXN3 and RECK 3'UTR's by miR-135b.* Changes in the normalized reporter gene activities of wild-type (WT) and mutant (MUT) *FOXN3* (left) and *RECK* (right) 3'-UTR luciferase reporter constructs in response to the co-transfection of negative control (NC) or miR-135b mimics in HEK293T cells. $^{**}p< 0.01$, $^{***}p< 0.001$, n.s., not significant.

Figure S11. *The effects of FOXN3 and RECK RNAi knockdown on cell proliferation.* SNU-638 cells were transfected with siRNA against *FOXN3* or *RECK*; or Control siRNA and their effects on cellular proliferation were measured. Data from two separate experiments are shown where values were normalized against those of Control and presented as mean ± SEM.

Figure S12. *Correlation of miR-135b target genes and Il1b expression levels.* (A) Correlation of relative *Foxn3* (top) and *Reck* (bottom) expression levels with those of *Il1b* in WT, *K19-C2mE* and *Gan* samples. (B) Correlation of relative *FOXN3* (top) and *RECK* (bottom) expression levels with those of *IL1B* in the TCGA human stomach adenocarcinoma (STAD) data set.

Figure S13. *Detection of miR-135b in cell culture supernatant.* The presence of miR-135b in the culture supernatant of untransfected MNK74 cells (Control) or MKN74 cells stably expressing miR-135b (miR-135b) was measured by qRT-PCR. Data are expressed relative to control values and presented as mean ± SD; ***$p<0.001$.

Supplementary Table S1. Oligonucleotide primers used for various studies as indicated.

Purpose	Gene symbols		Sequence (5' to 3')
Gene expression	Human *IL-1b*	Forward	CCAGGGACAGGATATGGAGCA
		Reverse	TTCAACACGCAGGACAGGTACAG
	Mouse *IL-1b*	Forward	TCCAGGATGAGGACATGAGCAC
		Reverse	GAACGTCACACACCAGCAGGTTA
	Human *FOXN3*	Forward	TCGTTGTGGTGCATAGACCC
		Reverse	GTGGACCTGATGTGCTTTGATA
	Human *RECK*	Forward	AGCAACCGAGCCCGTATGT
		Reverse	CCGAGTAGGCAGCACACACA
	Mouse *Foxn3*	Forward	TGCCCGACATCCGATTAGAAG
		Reverse	CTAAGGACCGACTCCCCAAAG
	Mouse *Reck*	Forward	AGATAACCAAATGTGCCGTGAT
		Reverse	TCAACCATTGTTTCAGGGCAATA
PCR primers for cloning into expression vectors	Human miR-135b cloning	Forward	CCGCTCGAGTTTATGGCCAGGAAG
		Reverse	CGGGATCCAAGGTCTCCTTCCTT
	Mouse miR-135b cloning	Forward	AAAGAGCTCAGAGGAGAGGGCAGTTAGGG
		Reverse	AAGGTACCGCCTAACCCTTCAGAACGAA
PCR primers for the construction of reporter gene constructs	FOXN3 3'-UTR	Forward	AAAGAGCTCATTTTTAAAGGAGATTGAAGCCATAGAAC
		Reverse	AAAACTCGAGTTCAGGCTTATGGCTTTTGG
	FOXN3 3'-UTR MUT1	Forward	AAAGAGCTCATTTTTAAAGGAGATTGAATTTTTAGAACTCATA
		Reverse	AAAACTCGAGTTCAGGCTTATGGCTTTTGG
	FOXN3 3'-UTR MUT2	Forward	AAAGAGCTCATTTTTAAAGGAGATTGAAGCCATAGAAC
		Reverse	AAAACTCGAGTTCAGGCTTAAAAATTTTGGAACA
	FOXN3 3'-UTR MUT1,2	Forward	AAAGAGCTCATTTTTAAAGGAGATTGAATTTTTAGAACTCATA
		Reverse	AAAACTCGAGTTCAGGCTTAAAAATTTTGGAACA
	RECK 3'-UTR	Forward	TATTTTATTATGAAGAAGGTGAATAGCCATATTTG
		Reverse	TCGACAAATATGGCTATTCACCTTCTTCATAATAAAATAAGCT
	RECK 3'-UTR MUT	Forward	TATTTTATTATGAAGAAGGTGAATATTTATATTTG
		Reverse	TCGACAAATATAAATATTCACCTTCTTCATAATAAAATAAGCT

Supplementary Table S2. List of differentially expressed microRNA as determined by microarray analysis of wild type and *Gan* tumor epithelial cells

Wild type (n=4), Gan (n=4)					
WT>Gan		WT<Gan			
Downregulated		Upregulated			
Genes	Log_{10}	Genes	Log_{10}	Genes	Log_{10}
mmu-miR-7b	-2.88	**mmu-miR-135b**	3.17	mmu-miR-21	0.87
mmu-miR-129-2-3p	-2.63	mmu-miR-218	2.66	mmu-miR-574-3p	0.85
mmu-miR-127	-2.58	mmu-miR-155	2.56	mmu-miR-5099	0.79
mmu-miR-133a	-2.32	mmu-miR-34b-5p	2.48	mmu-miR-362-5p	0.76
mmu-miR-224	-2.20	mmu-miR-669l	2.41	mmu-miR-153	0.76
mmu-miR-3085-3p	-1.82	mmu-miR-139-5p	2.36	mmu-miR-183	0.72
mmu-miR-3474	-1.68	mmu-miR-466m-5p	2.33	mmu-miR-205	0.70
mmu-miR-181d	-1.49	mmu-miR-3067*	2.23	mmu-miR-141*	0.67
mmu-miR-133b	-1.43	mmu-miR-28c	2.22	mmu-miR-22*	0.65
mmu-miR-214	-1.29	mmu-miR-3096b-5p	2.21	mmu-miR-3069-3p	0.62
mmu-miR-145	-0.97	mmu-miR-3096-5p	2.11	mmu-miR-33	0.59
mmu-miR-152	-0.84	mmu-miR-34c	2.09	mmu-miR-429	0.59
mmu-miR-34a	-0.82	mmu-miR-468	2.06	mmu-miR-672	0.57
mmu-miR-494	-0.78	mmu-miR-669e	2.04	mmu-miR-200a*	0.57
mmu-miR-10b	-0.75	mmu-miR-3070b-3p	2.03	mmu-miR-5130	0.56
mmu-miR-503	-0.72	mmu-miR-32*	2.00	mmu-miR-200b	0.56
mmu-miR-582-5p	-0.69	mmu-miR-3058	1.98	mmu-miR-200a	0.56
mmu-miR-143	-0.65	mmu-miR-466h-5p	1.96	mmu-miR-210	0.55
mmu-miR-1a	-0.61	mmu-miR-669b	1.95	mmu-miR-96	0.54
mmu-miR-7a	-0.55	mmu-miR-669o-5p	1.94	mmu-miR-200b*	0.52
mmu-miR-199a-3p	-0.55	mmu-miR-21*	1.91	mmu-miR-192	0.52
mmu-miR-199a-5p	-0.54	mmu-miR-128	1.89	mmu-miR-28	0.51
mmu-miR-375	-0.54	mmu-miR-484	1.86	mmu-miR-31*	0.48
mmu-miR-199b*	-0.49	mmu-miR-29c*	1.85	mmu-miR-1198-5p	0.47
mmu-miR-193	-0.48	mmu-miR-3068*	1.83	mmu-miR-148b	0.45
mmu-miR-378	-0.47	mmu-miR-703	1.78	mmu-miR-22	0.42
mmu-miR-130a	-0.46	mmu-miR-134	1.78	mmu-miR-1839-3p	0.42
mmu-miR-5105	-0.43	mmu-miR-5117	1.77	mmu-miR-5113	0.42
mmu-miR-10a	-0.42	mmu-miR-32	1.71	mmu-miR-331-3p	0.42
mmu-miR-181b	-0.41	mmu-miR-877*	1.66	mmu-miR-31	0.41
mmu-miR-378b	-0.40	mmu-miR-147	1.64	mmu-miR-690	0.40

mmu-miR-466h-3p	-0.40	mmu-miR-3110*	1.64	mmu-miR-194	0.40
mmu-miR-195	-0.37	mmu-miR-744	1.63	mmu-miR-200c	0.39
mmu-miR-378*	-0.35	mmu-miR-1196	1.59	mmu-miR-770-3p	0.39
mmu-miR-1306-3p	-0.34	mmu-miR-183*	1.56	mmu-miR-3082-5p	0.39
mmu-miR-132	-0.34	mmu-miR-5131	1.53	mmu-let-7b	0.37
mmu-miR-370	-0.33	mmu-miR-678	1.52	mmu-miR-425	0.36
mmu-miR-5115	-0.33	mmu-miR-28*	1.51	mmu-let-7c	0.36
mmu-miR-497	-0.31	mmu-miR-24-2*	1.50	mmu-miR-146a	0.34
mmu-miR-3472	-0.31	mmu-miR-532-3p	1.46	mmu-miR-23a	0.34
		mmu-miR-760-3p	1.44	mmu-miR-141	0.33
		mmu-miR-1967	1.38	mmu-miR-705	0.33
		mmu-miR-3075	1.38	mmu-miR-1839-5p	0.32
		mmu-miR-872	1.19	mmu-miR-3099	0.32
		mmu-miR-714	1.15	mmu-miR-24	0.32
		mmu-miR-192*	1.15	mmu-miR-103	0.32
		mmu-miR-466g	1.09	mmu-miR-669n	0.32
		mmu-miR-455	1.08	mmu-miR-652	0.31
		mmu-miR-1940	1.05	mmu-miR-182	0.31
		mmu-miR-296-5p	0.92	mmu-miR-15b	0.30

Supplementary Table S3. Candidate miRNAs predicted based on combined analyses of two microRNA profiles generated from wild type, *K19-C2mE* and *Gan* samples

WT (E^a,M^b) > Gan (E,M) & C2mE (M)		WT (E,M) < Gan (E,M) & C2mE (M)	
Downregulated		**Upregulated**	
Genes	**Log_{10}**	**Genes**	**Log_{10}**
mmu-miR-7b	-2.88	**mmu-miR-135b**	3.17
mmu-miR-129-3p	-2.63	mmu-miR-155	2.56
mmu-miR-127	-2.58	mmu-miR-34b-5p	2.48
mmu-miR-133a	-2.32	mmu-miR-139-5p	2.36
mmu-miR-224	-2.20	mmu-miR-34c	2.09
mmu-miR-145	-0.97	mmu-miR-32	1.71
mmu-miR-152	-0.84	mmu-miR-21	0.87
mmu-miR-34a	-0.82	mmu-miR-205	0.70
mmu-miR-7a	-0.55	mmu-miR-22*	0.65
mmu-miR-375	-0.54	mmu-miR-429	0.59
mmu-miR-378	-0.47	mmu-miR-672	0.57
mmu-miR-378*	-0.35	mmu-miR-200a*	0.57
		mmu-miR-200a	0.56
		mmu-miR-200b	0.56
		mmu-miR-200b*	0.52
		mmu-miR-192	0.52
		mmu-miR-194	0.40
		mmu-miR-425	0.36

[a]E, Epithelial cells; [b]M, Mixed cells

REFERENCES FOR SUPPLEMENTARY MATERIAL

1. Schneider CA, Rasband WS, Eliceiri KW. NIH Image to ImageJ: 25 years of image analysis. Nat Methods 2012;9:671-5.
2. Oshima H, Ishikawa T, Yoshida GJ, et al. TNF-alpha/TNFR1 signaling promotes gastric tumorigenesis through induction of Noxo1 and Gna14 in tumor cells. Oncogene 2014;33:3820-9.
3. Rogers AB. Histologic scoring of gastritis and gastric cancer in mouse models. Methods Mol Biol 2012;921:189-203.
4. Barker N, Huch M, Kujala P, et al. Lgr5(+ve) stem cells drive self-renewal in the stomach and build long-lived gastric units in vitro. Cell Stem Cell 2010;6:25-36.
5. Gerstein MB, Kundaje A, Hariharan M, et al. Architecture of the human regulatory network derived from ENCODE data. Nature 2012;489:91-100.
6. Wang J, Zhuang J, Iyer S, et al. Sequence features and chromatin structure around the genomic regions bound by 119 human transcription factors. Genome Res 2012;22:1798-812.